

Recent Advances in Oxidation Stable Chemistry of 2D MXenes

Fangcheng Cao, Ye Zhang,* Hongqing Wang, Karim Khan, Ayesha Khan Tareen, Wenjing Qian, Han Zhang,* and Hans Ågren*


As an emerging star of 2D nanomaterials, 2D transition metal carbides and nitrides, named MXenes, present a large potential in various research areas owing to their intrinsic multilayer structure and intriguing physico-chemical properties. However, the fabrication and application of functional MXene-based devices still remain challenging as they are prone to oxidative degradation under ambient environment. Within this review, the preparation methods of MXenes focusing on the recent investigations on their thermal structure–stability relationships in inert, oxidizing, and aqueous environments are systematically introduced. Moreover, the key factors that affect the oxidation of MXenes, such as, atmosphere, temperature, composition, microstructure, and aqueous environment, are reviewed. Based on different scenarios, strategies for avoiding or delaying the oxidation of MXenes are proposed to encourage the utilization of MXenes in complicated environments, especially at high temperature. Furthermore, the chemistry of MXene-derived oxides is analyzed, which can offer perspectives on the further design and fabrication of novel 2D composites with the unique structures of MXenes being preserved.

F. Cao, Y. Zhang, H. Wang
 Lab of Optoelectronic Technology for Low Dimensional Nanomaterials
 School of Chemistry and Chemical Engineering
 University of South China
 Hengyang 421001, China
 E-mail: yezhang@usc.edu.cn

K. Khan, A. K. Tareen, H. Zhang
 Shenzhen Engineering Laboratory of Phosphorene and Optoelectronics
 College of Physics and Optoelectronic Engineering
 Shenzhen University
 Shenzhen 518060, China
 E-mail: hzhang@szu.edu.cn

W. Qian
 School of Materials Science and Engineering
 Tongji University
 Shanghai 201804, China

H. Ågren
 Department of Physics and Astronomy
 Uppsala University
 Box 516, Uppsala SE-751 20, Sweden
 E-mail: hans.agren@physics.uu.se

 The ORCID identification number(s) for the author(s) of this article can be found under <https://doi.org/10.1002/adma.202107554>.

© 2022 The Authors. Advanced Materials published by Wiley-VCH GmbH. This is an open access article under the terms of the Creative Commons Attribution-NonCommercial License, which permits use, distribution and reproduction in any medium, provided the original work is properly cited and is not used for commercial purposes.

DOI: 10.1002/adma.202107554

1. Introduction

2D transition metal (TM) carbides and carbonitrides (named MXenes) have since their first appearance in 2011 drawn great attention in various application fields owing to their combination of 2D layered structure and excellent physico-chemical properties.^[1] MXenes can be derived from the corresponding laminated MAX phases that are governed from the formula $M_{n+1}AX_n$ ($n = 1-3$).^[2] MAX phase compounds consist of transition metal (M) layers that interleave C or N layers (X), and the strong M–X bonds are further intercalated by monatomic layers of group III A or IV A elements (A), showing an atomic-layer and hexagonal-crystal structure.^[3,4] Normally, MXenes can be achieved by preferentially dissolving and extracting the weakly bonded A layers from the structure of the MAX phases.^[5,6] During etching

and exfoliation in the aqueous phase, the highly reactive TM surfaces are immediately linked with species like $-F$, $-OH$, and $=O$, resulting in the MXene general formula: $M_{n+1}X_nT_x$ (T_x represents surface species).^[7-9] Based on the abundant surface terminations, unique layered structures with mixed covalent and metallic bonding, MXenes present intriguing functional performance, such as, excellent electrochemical and optical properties, superior thermal conductivity, high electrical conductivity, and outstanding mechanical characteristics.^[10-13] These properties of MXenes can be further modulated by variations in microstructure, element composition, and surface terminations,^[14-19] for example, by varying M or X elements, alloying M or X layers,^[20-24] and constructing special vacancy in MXene structures by using multi-elements (M) out-of-plane or in-plane order.^[23,25-29] Therefore, the versatile and potentially scalable synthesis technologies render the MXene materials a distinctive position in the 2D materials community with tunable properties.^[30]

To date, almost 30 diverse MXenes have been successfully experimentally fabricated. The configuration and corresponding properties of several MXenes have been theoretically predicted, mostly by applying density functional theory (DFT). The experimental and theoretical reported MXenes consist of Ti_2C , Ti_3C_2 , Ta_4C_3 , Ti_3CN , $TiNbC$, $TiCr_2C_2$ etc.,^[31-33] as summarized in **Figure 1**. Moreover, it is assumed that more novel and promising MXenes will be designed and obtained

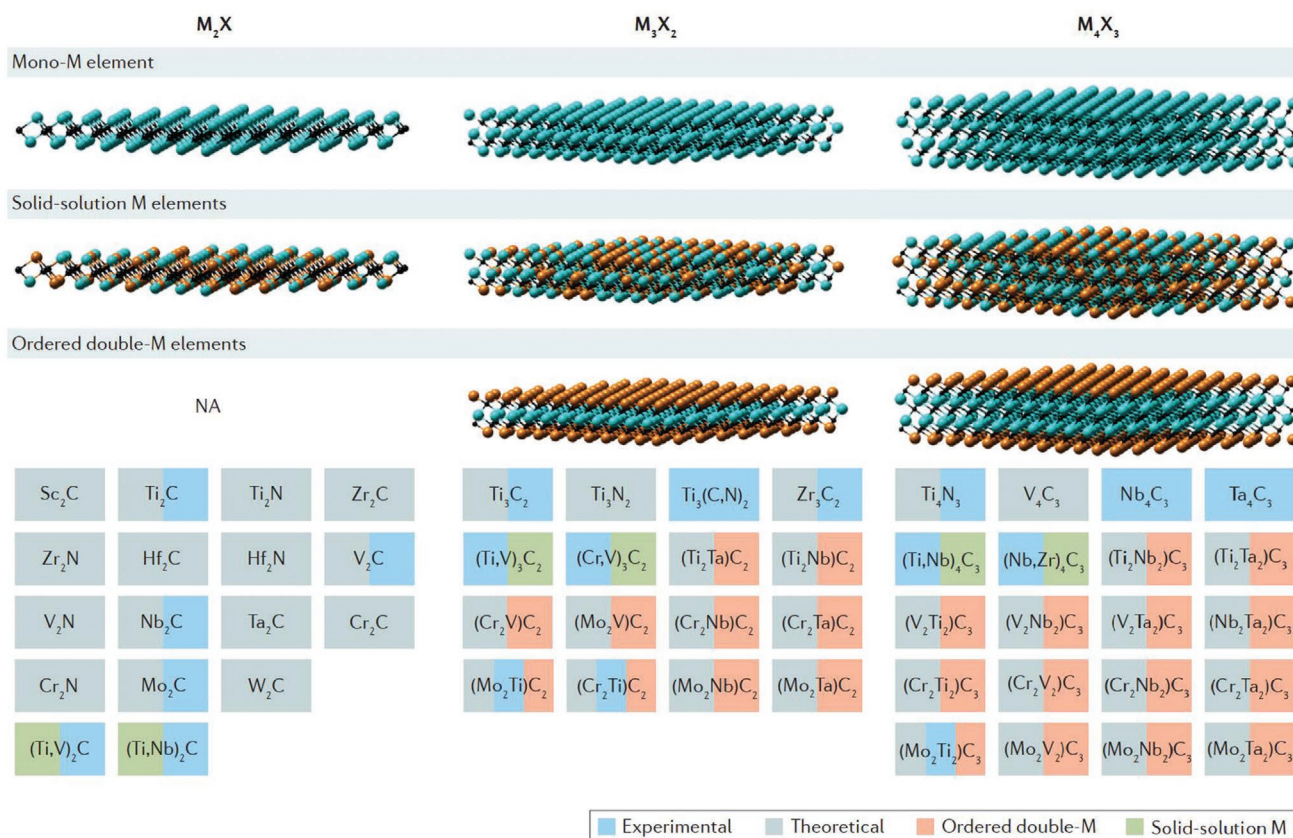


Figure 1. Summary of experimental and theoretical reported MXenes in the formula of $M_{n+1}X_n$ ($n = 1-3$), including mono-M elements and a solid solution of multi-M elements. Reproduced with permission.^[31] Copyright 2017, Springer Nature.

from their respective MAX materials, attributing to the large family of MAX phases.^[34–36] With the increasing attraction to the unprecedented development of MXene materials, several reviews have reported their preparation methods, physical and chemical properties, as well as potential applications.^[8,37] Very recently, Naguib et al., gave a historical overview of the first 10 years of MXene research and provided a perspective on their synthesis and future development.^[38] The continuous development of environmentally friendly, safe, efficient, and scalable synthesis approaches was shown fundamental to achieve enhanced MXenes with desired properties. Additionally, the novel opto-electro-magnetic properties and emerging applications of MXenes have recently attracted growing interest.^[39,40] For optimizing the properties of pristine MXene, the previous reviews have focused on theoretical simulations, synthesis, and applications of hetero-MXenes and MXene-based composites.^[41–43] According to previous publications, pristine MXenes, hetero-MXenes and MXene-based composites can be successfully applied in many areas, such as energy-storage materials,^[44–46] reinforcing fillers,^[47–49] electromagnetic interference shielding,^[50–52] sensors,^[53–56] and catalysts.^[57–61] But in practice, the fabrication and application of functional MXene-based devices still remain challenging as they are prone to oxidative degradation under ambient environment. A lot of studies have demonstrated that MXene nanosheets (NSs) have poor chemical durability in water and in ambient conditions due to the

structural transformation caused by collective effects from air, moisture, and light, resulting in unwanted oxidation and degradation of the properties.^[62–67] Similarly, MXene films exposed to atmospheric air can also undergo oxidation.^[68,69] These types of degradation might severely destroy the structure integrity, which further limits the lifetime and precludes many useful properties of MXene-based devices for future applications. However, few reviews have provided a comprehensive summary of the degradation mechanism and oxidation chemistry for both MXenes and MXene-derived oxides.

In this review, we systematically highlight recent progress on the oxidation stable chemistry of MXenes. After giving a brief introduction of preparation techniques of MXenes, the structure evolution and phase transition of MXenes during the oxidation process are analyzed to reveal the oxidation mechanism and kinetics of MXenes. The effects of atmosphere (air, O₂, CO₂, etc.), temperature, composition, surface termination groups, defects, and aqueous environment on the degradation of MXenes are analyzed. Moreover, strategies that can endow MXenes with antioxygenic characteristics, extended lifetime, and stable functional properties in different conditions are highlighted. We also discuss the development of in situ synthesized MXene-derived oxide hybrids. This review thus aims to present some perspectives for the challenges and opportunities of the oxidation chemistry of MXenes, which can bring new research significance to the protection and application of MXenes.

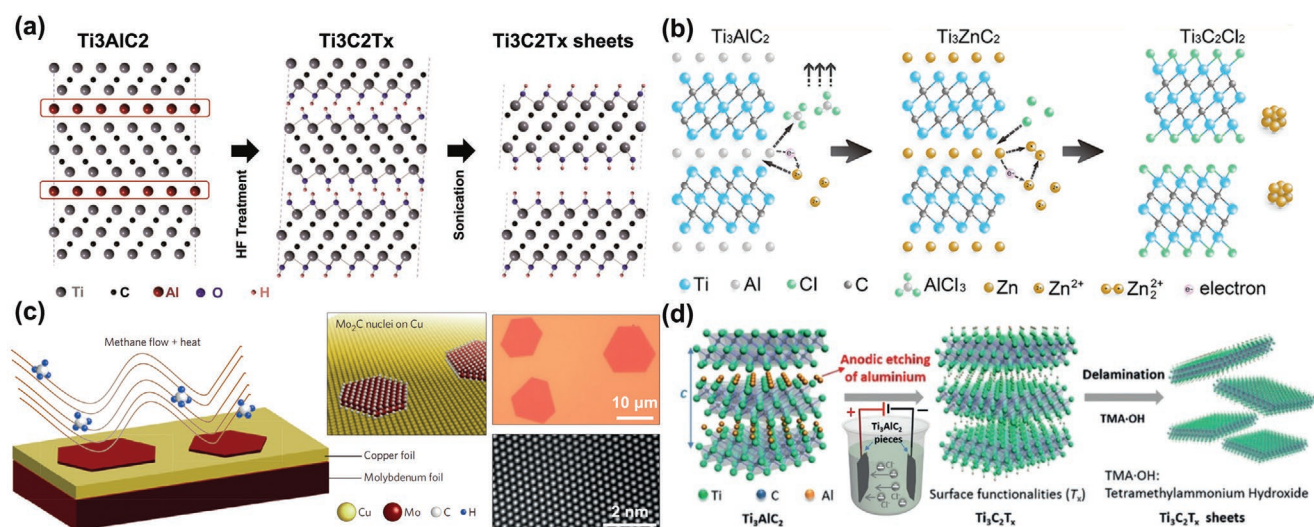
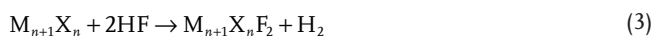
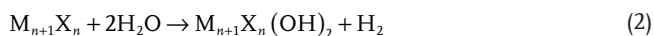
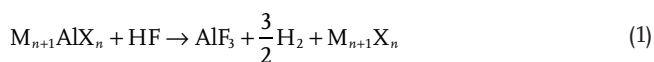


Figure 2. Schematic fabrication processes of MXenes. a) Wet chemical etching. Reproduced with permission.^[1] Copyright 2011, Wiley-VCH. b) Molten salts etching. Reproduced with permission.^[70] Copyright 2019, American Chemical Society. c) Chemical vapor deposition. Reproduced with permission.^[71] Copyright 2015, Springer Nature. d) Electrochemical etching. Reproduced with permission.^[72] Copyright 2018, Wiley-VCH.

2. Synthesis Methods of MXenes

2D MXene nanomaterials were first synthesized via immersing Al-containing MAX phases in hydrofluoric acid (HF), and then Al atoms with comparatively weak bonding were selectively dissolved.^[1] Various methods have been applied to prepare MXenes, for instance, wet chemical etching, molten salts etching, chemical vapor deposition (CVD), and electrochemical etching.^[37,70–72] Figure 2 illustrates the typical fabrication processes of MXenes from different routes. Monolayer or few-layered MXene NSs can be further derived by ultrasonic treatment or molecule intercalation from multi-layered MXene structures.^[73–75] The experimental parameters applied when etching and delamination significantly affect the shape, size, morphology, and surface chemistry of MXene NSs, and thereby determine the processing and performance of the MXenes.^[8,76–79]

Wet chemical etching is one of the most commonly applied approaches to prepare MXenes. Most of the MAX layers will be separated after immersing in HF solution with the emergence of $-\text{OH}$ and $-\text{F}$ terminal species, which can be expressed by the reactions below:^[1]



During wet chemical etching the Al is gradually removed, causing the delamination of MAX, and further making the stacked NSs into thinner layers. Usually, the HF etched multi-layer MXene NSs show a small lateral size with severe defects in the structure.^[16,80,81] To obtain desired MXene NSs with large lateral size and fewer defects, modified methods by using mixed lithium fluoride-hydrochloric acid (LiF-HCl), or bifluoride (e.g., NH_4HF_2 , NaHF_2 , and KHF_2) etching solution have

been proposed.^[82–85] Figure 3 compares the effects of different etching parameters on the morphology of MXene NSs. MXene NSs produced by traditional procedure (Route 1 in Figure 3) show here smaller size and irregular edges distributed with small dark particles and numerous pinholes. In comparison, the MAX phase could be delaminated without breaking the NSs that were visually hole-free with clearly-defined and clean edges by using the optimized process (Route 2 in Figure 3). In this case, multilayer MXene NSs can be easily separated to monolayer NSs by manual shaking instead of sonication that usually shred NSs into smaller pieces.

Another normally adopted method to prepare MXenes is using molten fluoride salts, Lewis acid or Lewis-base salts (e.g., LiF , NaF , and ZnCl_2) at high temperatures, which can tune the functional terminals on the MXene surface by choosing different compositions of the molten salts.^[70,86,87] For example, Li et al., successfully synthesized $\text{Ti}_3\text{C}_2\text{Cl}_2$ and Ti_2CCl_2 MXenes by delamination of Ti_3ZnC_2 and Ti_2ZnC in molten ZnCl_2 , as shown in Figure 2b.^[70] The Cl-terminated MXenes are shown to exhibit better stability with enhanced electrochemical performance than the F-terminated ones, which has inspired the design of the surface functional terminals on MXenes with improved oxidation stability for a variety of future applications.^[88–90] Recently, the CVD method was explored to produce ultrathin MXenes, such as Mo_2C , WC , and TaC NSs.^[71,91,92] For example, the perfect crystals of $\alpha\text{-Mo}_2\text{C}$ could be grown on a combination substrate of copper foil and molybdenum foil via CVD in methane atmosphere, as illustrated in Figure 2c.^[92] MXenes obtained by the CVD based process, often exhibit a large area (over $100\ \mu\text{m}$ in lateral size), high quality (high crystallinity and defect-free) with no terminations, which provides opportunities for investigations of the intrinsic properties of the MXenes. Electrochemical etching, which is a feasible HF-free technique with milder reaction conditions, has been regarded as a potential green method for preparing MXenes, as shown in Figure 2d.^[72,88,93–95] Because Al is in a more oxidized state than M in the MAX phase, the Al layers tend to be

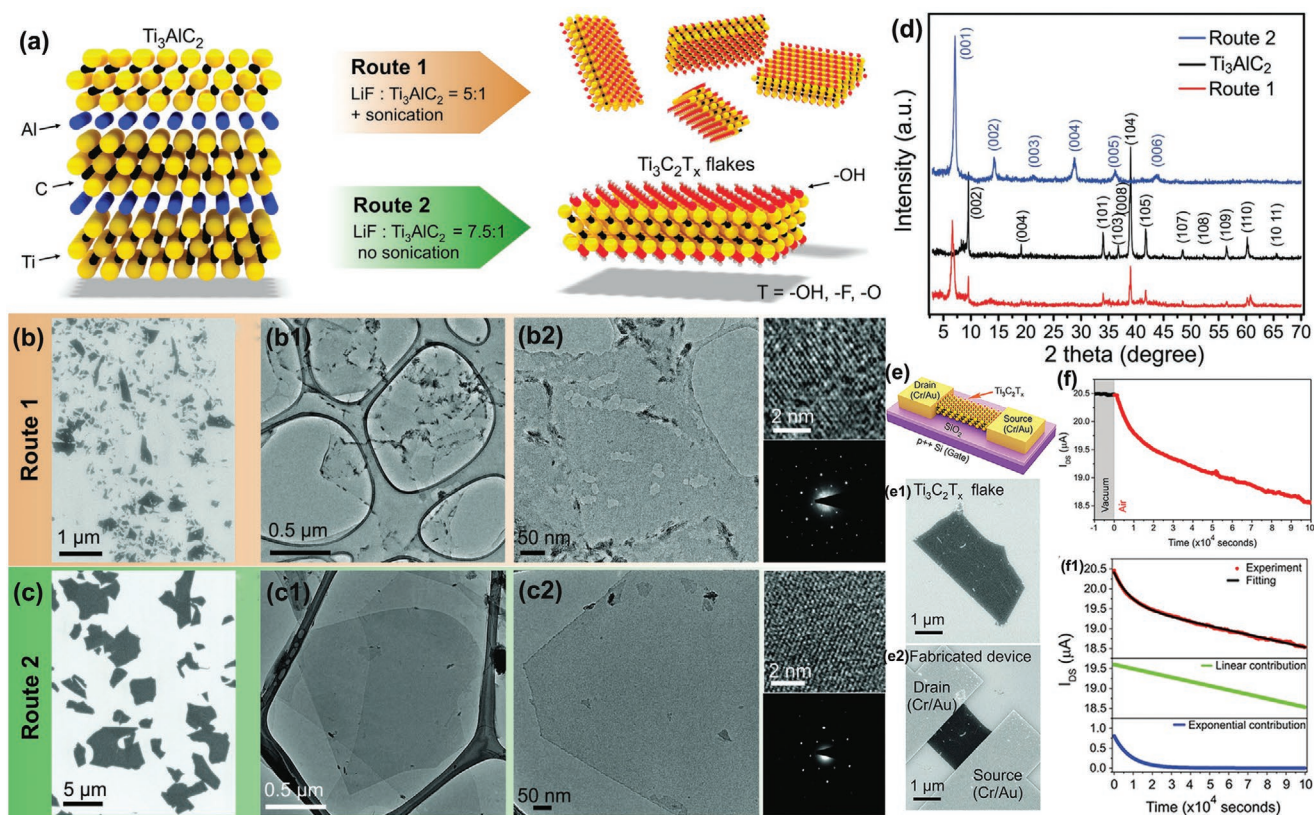


Figure 3. a–d) The diagrams, SEM images, TEM images, SAED patterns, and XRD patterns of $\text{Ti}_3\text{C}_2\text{T}_x$ NSs produced by Routes 1 and 2. e) Diagram and SEM images of device fabrication of $\text{Ti}_3\text{C}_2\text{T}_x$ -based FET. f) The correlation between drain-source current (I_{DS}) and time (t) for $\text{Ti}_3\text{C}_2\text{T}_x$ FET measured in air, and fitting of the $I_{\text{DS}}-t$ relationship which can represent the oxidation degradation law. Reproduced with permission.^[82] Copyright 2016, Wiley-VCH.

more easily extracted during electrochemical processes. The proper etching parameters like voltage, time, and temperature are necessary for preventing over-etched MAX phases through the formation of carbide-derived C.^[94] For example, Sun et al., effectively prepared Ti_2CT_x in HCl solution at 0.6 V for 120 h based on the electrochemical etching method.^[88] Moreover, the in situ formed MXenes on electrode surfaces through an electrochemical process is not only a green and facile fabrication technique of MXenes-devices, but also possesses unique advantages for electrocatalytic applications. Li et al., for example, in situ constructed a V_2CT_x MXene-based zinc ion battery via electrochemical method with a MAX cathode in an etchant contained electrolyte, which exhibited excellent cycling stability and rate performance.^[95]

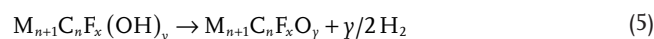
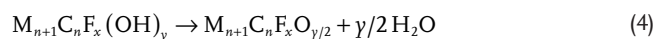
3. Thermal Stability and Oxidation Mechanism of MXenes

As the high surface area to body mass ratio, 2D nanomaterials are extremely sensitive to environment with poor thermal stability, among which MXenes are among the worst in this category.^[96–98] Thermal stability and structural integrity are especially important because MXenes may undergo various heat-treating operations in the preparation process, as well as, in their application environments.^[67] Furthermore, the thermal instability is a critical issue that severely hinders the large

industrial scale utilization of MXene materials.^[82,99] Therefore, it is urgent to study the stability of MXenes and clarify the changes of their structure and properties in different environments.

3.1. Thermal Stability and Structure Variation

Structural variations of MXenes occur during heat treatment in inert atmospheres at elevated temperatures primarily due to a combination of surface terminations and molecular hydrogen trapped between MXene NSs.^[97,100,101] Figure 4 summarizes the thermal analysis of $\text{Ti}_3\text{C}_2\text{T}_x$, Nb_2CT_x , and Mo_2CT_x based on thermal gravity (TG) and differential thermal gravity measurements. It can be seen that the mass of MXenes decreases with increasing temperature, which can be roughly divided into four stages. A gradual weight loss in the TG curve is observed from room temperature to about 400 °C (i.e., first stage), which is attributed to the desorption of van der Waals forced H_2O and HF in the MXene structure.^[102–104] The next stage (400–800 °C) is the remove of H_2O or H_2 in the form of $-\text{OH}$ groups occupied on the MXene NSs surface, according to the equation:^[99,105]



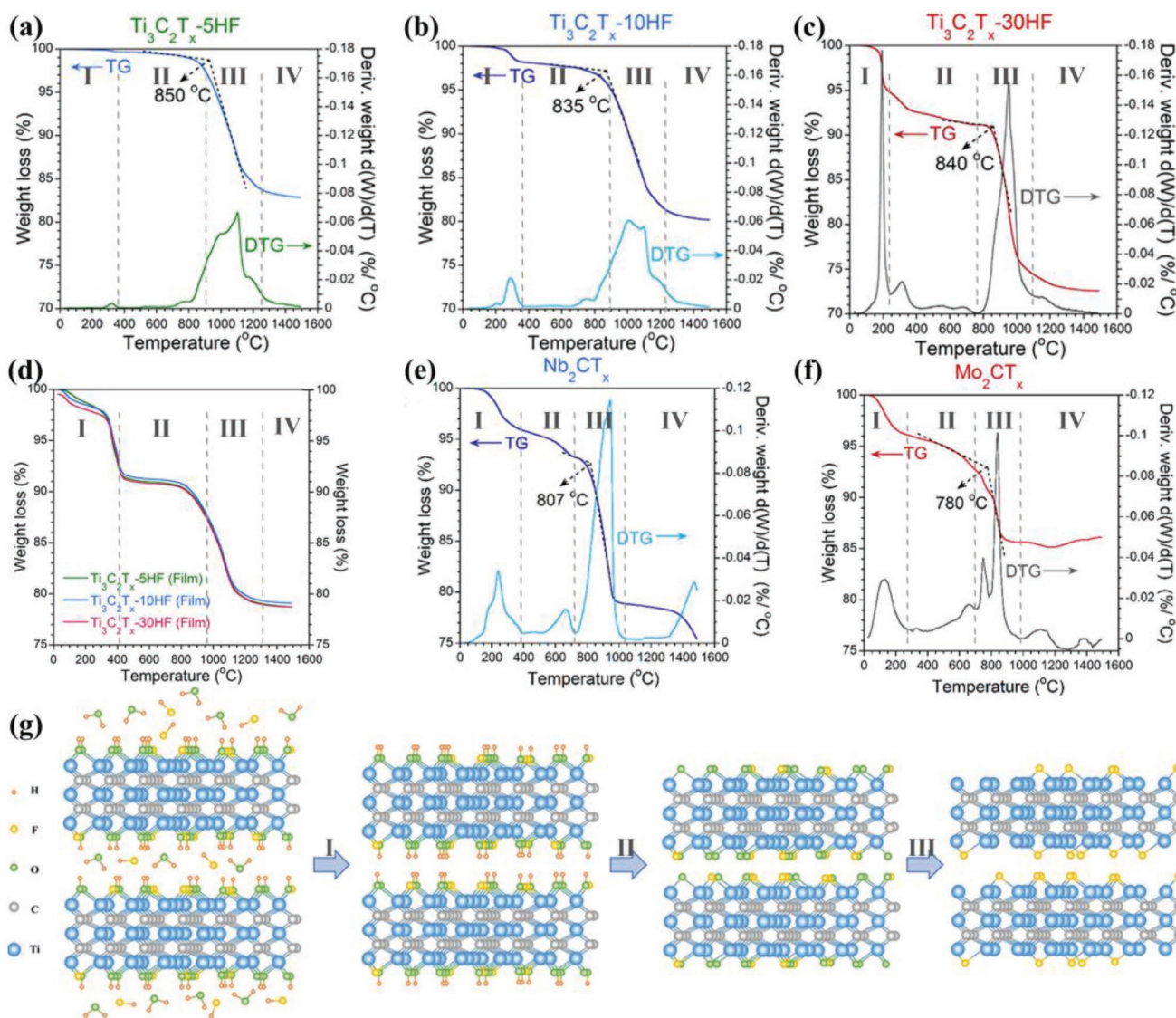
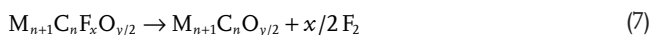
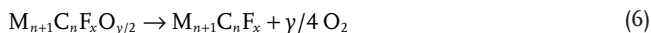


Figure 4. TG/DTG curves for a–d) Ti₃C₂T_x obtained by etching Ti₃AlC₂ using three different HF concentrations of 5, 10, and 30 wt%, e) Nb₂CT_x and f) Mo₂CT_x. Reproduced with permission.^[100] Copyright 2019, American Chemical Society. g) Diagram of a general rule for the structure variation of the MXenes.

With increasing heat treatment temperature (800–1100 °C), the surface –F or =O species start to disappear. According to the bonding energy, the elimination of =O would be more likely to occur than that of –F, following the below equation:^[97,106]



At higher temperature (>1200 °C), more =O and –F may be eliminated.^[107,108] Meanwhile, the heat treatment would induce crystal structure variation, such as interlayer spacing reduction, defect healing and twinning transformation.^[108–110] The collapse of layer structure would even occur in extreme conditions. The degradation temperature of MXenes strongly depends on their chemical composition and initial structure, but the structural

variation of different MXenes follows a general rule as illustrated in Figure 4f, which contains significant information for tuning and tailoring the surface functional groups and inter-layer distance of MXenes.

3.2. Oxidation Behavior and Processes

The oxidation of MXenes depends on the exposure to an oxidative environment. Persson et al., demonstrated that the =O terminations could eventually reach supersaturation at $x \approx 3.5$ with a retained Ti₃C₂T_x MXene NS structure.^[111,112] Many studies have reported the structural changes and phase transformation from MXenes to MXene/oxide NSs, C/oxide NSs, and final oxide products upon oxidation.^[113–115] For example, Li et al., studied the oxidation process of Ti₂CT_x in a CO₂ atmosphere—the

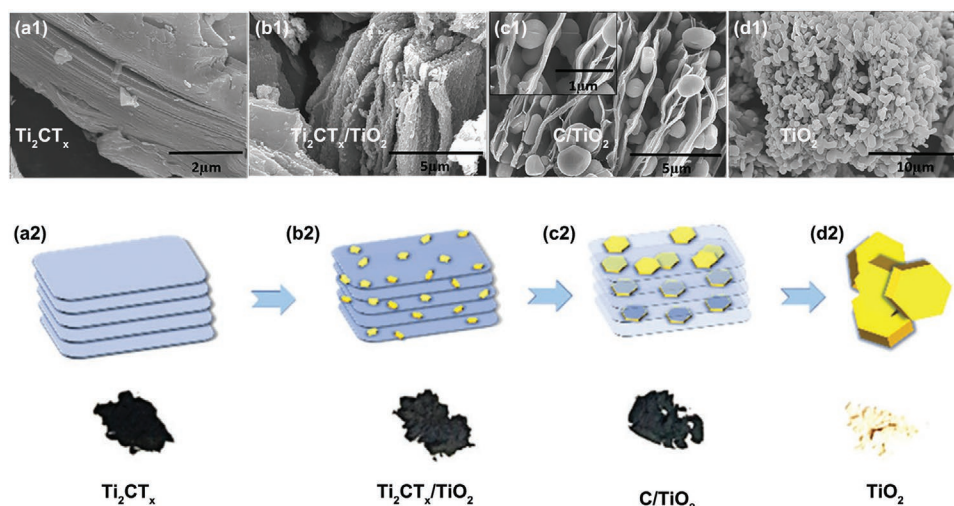


Figure 5. SEM images of a1) Ti_2CT_x , b1) $\text{Ti}_2\text{CT}_x/\text{TiO}_2$, c1) C/TiO_2 , and d1) TiO_2 with (a2–d2) showing the schematic structure evolution and phase transition of Ti_2CT_x during the oxidation process. Reproduced with permission.^[115] Copyright 2017, The Royal Society of Chemistry.

results are illustrated in **Figure 5**.^[115] The exterior or internal Ti layers were shown to react with CO_2 to create TiO_2 (i.e., a $\text{Ti}_2\text{CT}_x/\text{TiO}_2$ nanocomposite) when the temperature is low, with the smooth MXene NSs then becoming rough (Figure 5b1,b2). Thermodynamics and oxidation kinetics restrict this process, which can halt as a partial oxidation process. But it could gradually transform into a complete oxidation process as a result of the diffusion of CO_2 through newly formed TiO_2 as the temperature increases. When the Ti elements in Ti_3C_2 MXenes are consumed to form TiO_2 nanoparticles (NPs) accompanied by the transformation of anatase TiO_2 into the thermally stable rutile TiO_2 phase, the C elements left would spontaneously initiate the formation of a C layer. As a result, a C/TiO_2 hybrid structure is formed (Figure 5c1,c2). The exposed C layers continually oxidized under the adequate CO_2 environment until the C component is consumed completely, and there are only a rutile TiO_2 phase remaining (Figure 5d1,d2). This has stimulated the in situ synthesis of novel architectures of nanohybrid structures under well-controlled oxidation processes with the unique 2D layered structure of the MXenes retained. The chemical reactions equation of Ti_2CT_x with CO_2 can be described below:



MXene NSs cannot sustain prolonged exposure to an oxidizing atmosphere, particularly at high temperature, which may result in a nucleation phenomenon of oxides homogeneously decorated on the MXene NS surface. Moreover, based on in situ TEM analysis coupled with Raman spectroscopy techniques, Ghassemi et al., revealed the structural evolution of the oxides on $\text{Ti}_3\text{C}_2\text{T}_x$ surfaces in air.^[116] **Figure 6** shows the schematic oxidation mechanisms under different heating rates. For the flash oxidation regime, the ultrathin anatase TiO_2 NPs are first formed (Figure 6b1,b2), which subsequently shrink laterally and grow vertically into 3D particles (Figure 6c1,c2) via

inter-layer diffusion by Ostwald ripening that consumes the smaller particles, accompanied by the formation of disordered C. For the slow oxidation regime, the Ti layers transform into homogeneous NSs of nanocrystalline rutile (Figure 6d1,d2). It has been demonstrated that there is no intermediate anatase phase formed, and the rutile is directly generated from the Ti atoms. In addition, C layers with rearranged graphitic structures form under TiO_2 NSs due to the slow heating regime. Therefore, a desired phase composition and morphology of MXenes-derivatives can be achieved by manipulating the oxidation rate.

Figure 7 shows the microstructure of MXenes before and after oxidation. The nucleation of oxides can be observed homogeneously dispersed on MXene NSs during the oxidation process (Figure 7c). It has also been reported that oxide nanocrystals grow both between and at the edges of MXene NSs after oxidation.^[117,119,120] Differently, some results reported in literature have demonstrated that the oxidation of MXene NSs primitively occurs at the more vulnerable edges rather than on the basal plane (Figure 7b).^[63,82] The MXene oxidation mechanism has yet to be fully understood. **Figure 8** shows that the oxidation of $\text{Ti}_3\text{C}_2\text{T}_x$ colloidal solutions under ambient environment also started at the edges.^[63] With the advent of both dissolved O_2 and water in solution, the dissolved O_2 would preferably destroy the most susceptible edges of the MXene NSs to form TiO_2 (Figure 8d). It can be presumed that this degradation phenomenon could be substantially suppressed via removal of the dissolved O_2 from water through compressed inert gases.

3.3. Oxidation Kinetics

Previous studies have shown that oxidation with the passage of time bring performance degradation of MXene NSs (e.g., the electrochemical properties).^[121] So, it is especially imperative to explore and understand the oxidation kinetics of MXenes with the aim of predicting their performance degradation rate

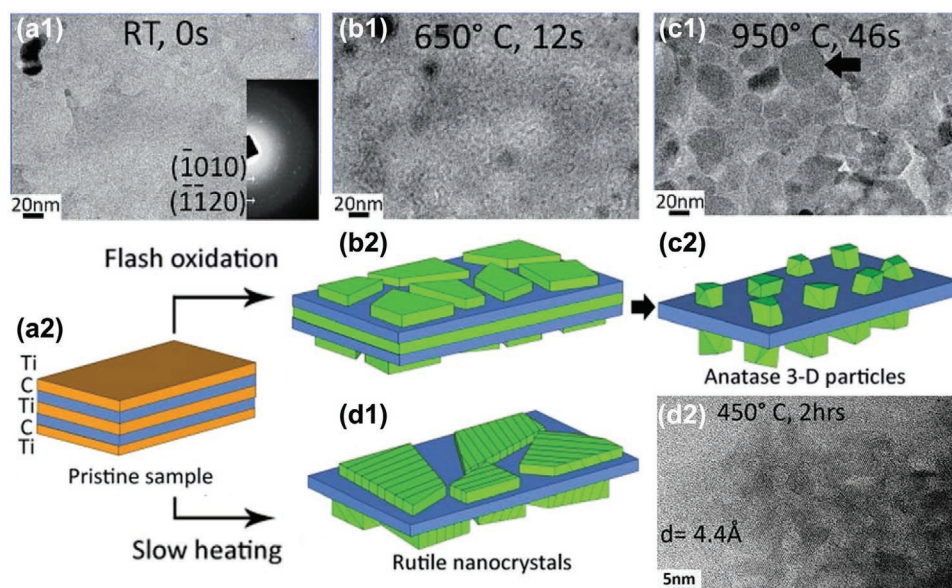


Figure 6. TEM images and schematic oxidation mechanism of $\text{Ti}_3\text{C}_2\text{T}_x$ under different heating rates: a1,a2) MXene with layered structure, b1,b2,c1,c2) representing the flash oxidation mechanism with the formation from ultrathin anatase NPs to 3D anatase NPs, d1,d2) showing a slow oxidation mechanism with rutile nanocrystals formed directly. Reproduced with permission.^[116] Copyright 2014, The Royal Society of Chemistry.

under an oxidation environment. Zhang et al., studied the oxidation kinetics of colloidal MXenes based on the concentration of MXene NSs over time as shown in Figure 8.^[63] They found out that the degradation behavior of MXenes is similar to that of aqueous solutions of black phosphorus and that it followed a single exponential decay behavior according to the empirical equation:^[63,122]

$$A = A_{\text{unre}} + A_{\text{re}} e^{-t/\tau} = A_{\text{unre}} + A_{\text{re}} e^{-kt} \quad (10)$$

where A , A_{unre} , and A_{re} represent the concentration, stable/unreactive, and reactive/unstable of MXene NSs, respectively; t , τ , and k represent the time, time constant (days), and rate constant, respectively. Thus, it is possible to estimate the concentration of MXene NSs at a certain time according to this degradation law. Based on the exponential decay law of Equation (10), the oxidation rates of aqueous $\text{Ti}_3\text{C}_2\text{T}_x$ or Ti_2CT_x suspensions has been comprehensively investigated under various environments, for instance different pH and temperature conditions as shown in Figure 9.^[66,123–125] These results confirm that a decreased pH or an increased temperature accelerate the oxidation rate. Furthermore, the activation energy of

the oxidation reaction can be calculated based on the Arrhenius equation as given below:^[66,123]

$$\ln k = \ln A - E_a/RT \quad (11)$$

where k is the rate constant, T is the temperature, A and E_a are the preexponential factor and the activation energy for the reaction, respectively, and R represents the universal gas constant. The activation energy increases with increasing pH, which suggests that a minimum energy is required to overcome the energy barrier for initiating the oxidation reaction under acidic conditions (Figure 9d3). Besides, Lipatov et al., indirectly studied oxidation kinetics of MXenes by measuring the conductivity change of field-effect transistors (FETs) based on a single-layer MXene NS versus time in air, as presented in Figure 3e.^[82] Based on the dependencies of drain-source current and time for $\text{Ti}_3\text{C}_2\text{T}_x$ FETs exposed to air, the degradation was found to be initially dominated by an exponential decay, but then the contribution of a linear decrease played a prominent role (Figure 3f). The exponential and linear combination oxidation kinetics presented by the correlation between drain-source current (I_{DS}) and time (t) can be described by the following equation:

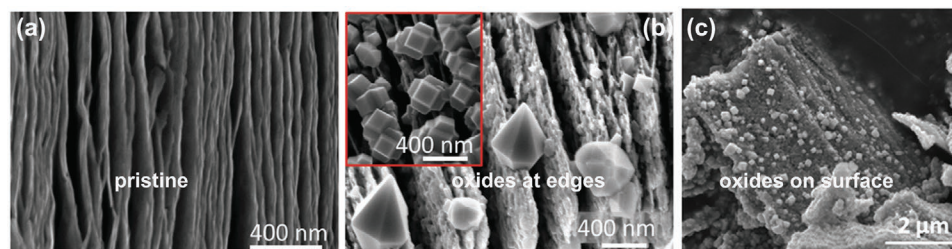


Figure 7. SEM microstructure of a) typical as-synthesized multilayer $\text{Ti}_3\text{C}_2\text{T}_x$, and b,c) $\text{Ti}_3\text{C}_2\text{T}_x$ after oxidation showing different oxidation morphology. b) Reproduced with permission.^[117] Copyright 2014, The Royal Society of Chemistry. c) Reproduced with permission.^[118] Copyright 2015, American Chemical Society.

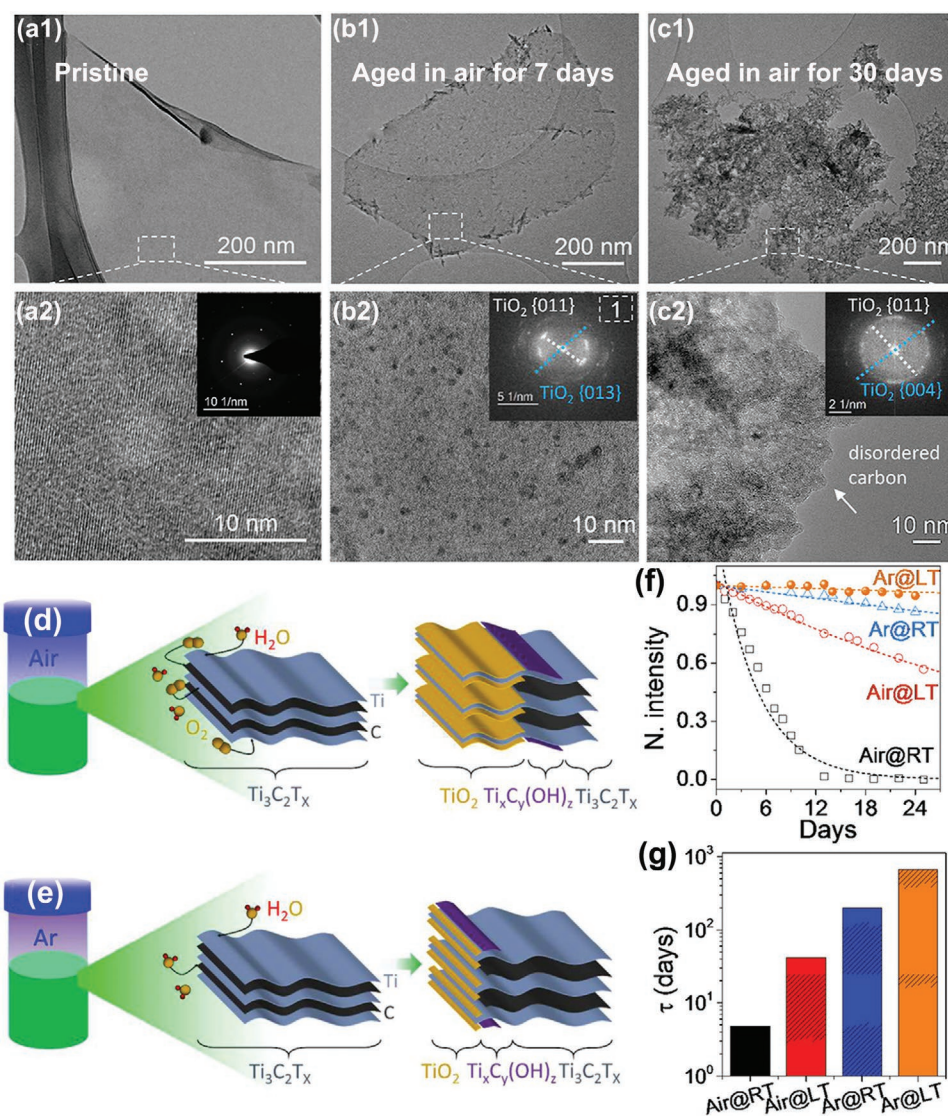


Figure 8. TEM microstructure of MXene NSs from a1,a2) as-prepared $\text{Ti}_3\text{C}_2\text{T}_x$ solutions and aged $\text{Ti}_3\text{C}_2\text{T}_x$ solutions at room temperature in Air for b1,b2) 7 days and c1,c2) 30 days, with inset showing the corresponding SAED pattern and FFT patterns, respectively, which are consistent with the schematic degradation of the MXene aqueous solutions starting at the edges in d) Air and e) Ar. f) The exponential decay and g) time constants of colloidal $\text{Ti}_3\text{C}_2\text{T}_x$ in different environments. Reproduced with permission.^[63] Copyright 2017, American Chemical Society.

$$I_{\text{DS}}(s) = A - B \times t + C \times \exp(-\gamma \times t) \quad (12)$$

where A, B, C, and γ are fitting constants. Based on this oxidation kinetics, the oxidation of $\text{Ti}_3\text{C}_2\text{T}_x$ NSs proceed quickly at first due to fully exposed edges to air. It is generally known from the oxidation kinetics of 3D materials that the oxidation products would passivate the whole material surface and then the oxidation rate reduces with the increasing thickness of the formed oxide layer. However, it is not the same case for the edge oxidation of 2D $\text{Ti}_3\text{C}_2\text{T}_x$. The TiO_2 produced at the sides of the $\text{Ti}_3\text{C}_2\text{T}_x$ NSs is not able to completely leave the material from the influence of an environment. Once the formation of oxides appeared at the NSs edges and the oxidation rate reduced to a specific level, the oxidation reaction would maintain at nearly a constant rate. At this stage, the oxidizing agents diffuse directly at the $\text{Ti}_3\text{C}_2\text{T}_x/\text{TiO}_2$ interface instead of through

the oxide layer like in the 3D materials case. More detailed research should be performed to reveal the applicability of the exponential and exponential-linear oxidation kinetics for other MXene materials in case of the oxidation mainly taking place at the edges or on the basal plane. It is clear that understanding the oxidation kinetics of MXenes is very important for stimulating fundamental academic studies, as well as, for the design of MXenes with improved oxidation stability for a variety of future applications.

4. Factors Affecting the Oxidation of MXenes

An in-depth understanding of the factors that affect the thermal stability is necessary for modulating the properties of MXenes through specific treatments so as to fulfill practical application

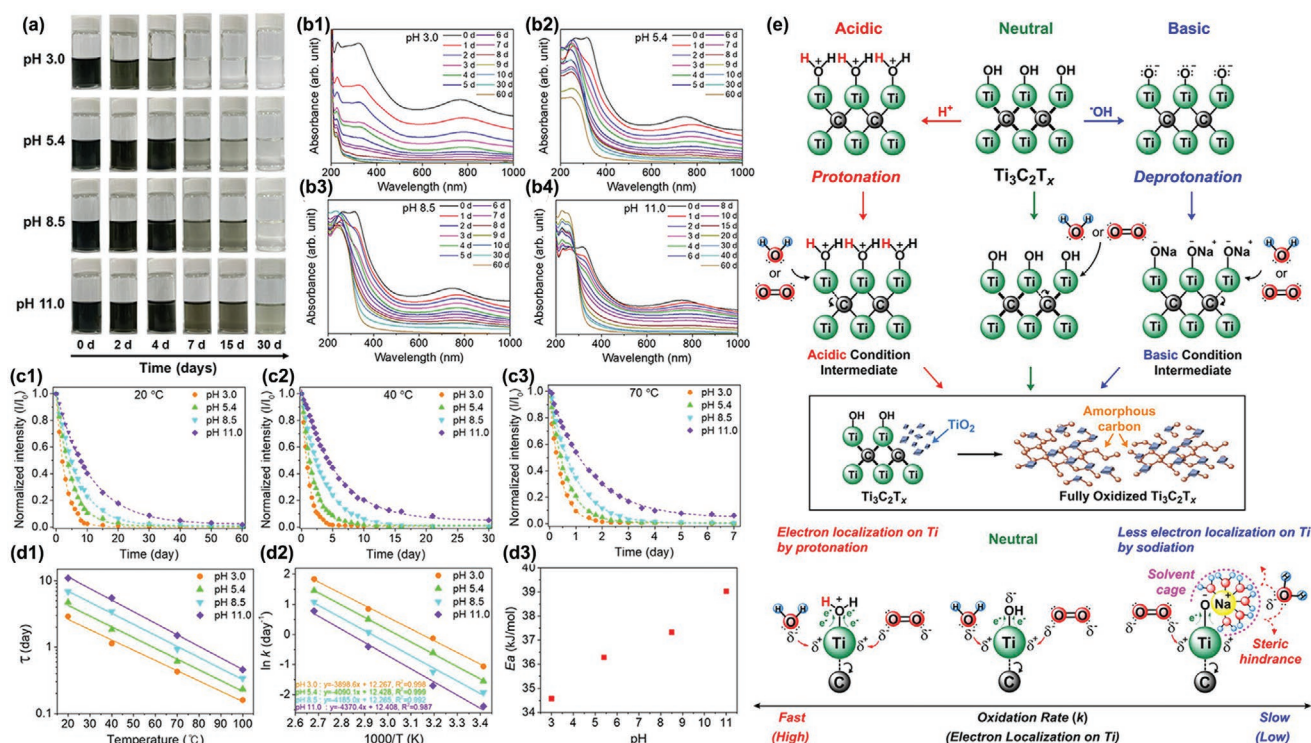


Figure 9. a) Digital photographs, b1–b4) UV–vis absorbance spectra, c1–c3) normalized intensity of the absorbance peak at 780 nm, d1–d3) rate constants and activation energy of aqueous $\text{Ti}_3\text{C}_2\text{T}_x$ suspensions. e) Proposed oxidation mechanism of $\text{Ti}_3\text{C}_2\text{T}_x$ colloids at different pH conditions. Reproduced with permission.^[123] Copyright 2021, American Chemical Society.

requirements. It has been demonstrated in earlier research works that the structural stability of MXenes is controlled by numerous key factors, involving chemical environment and intrinsic characteristics like atmosphere, temperature, composition, microstructure, and aqueous environment.^[31] The oxidation properties of MXenes with the same composition also varies a lot owing to the different synthesis methods and conditions. The basic relationship of the external and internal factors on the thermal stability of MXenes in preparation or operation (in situ) still requires to be explored so as to manufacture MXenes with required properties for high temperature utilization.

4.1. Atmosphere Environments

The structural and chemical stability of MXenes in vacuum, inert, oxidizing, or reducing atmosphere have been widely studied, among which Ti-based MXenes (e.g., $\text{Ti}_3\text{C}_2\text{T}_x$, Ti_2CT_x) belong to the most studied ones.^[97,99] It has been found that Ti_3C_2 MXenes are stable in Ar atmosphere at temperatures even up to 800 °C.^[97] However, in an O_2 atmosphere, they begin to oxidize with anatase homogeneously decorated on the surface at a low temperature (i.e., 200 °C), and then the further oxidation at 1000 °C would completely transform anatase to the rutile phase.^[97] The oxidation behavior in an NH_3 atmosphere was analogous to that in the inert atmosphere, the C atoms in MXenes, meanwhile, might be incompletely replaced by the N atoms to

form N-doped MXenes.^[126,127] For example, Wen et al., synthesized N-doped MXenes (1.7–20.7 at% surface N) by annealing $\text{Ti}_3\text{C}_2\text{T}_x$ at 200–700 °C in NH_3 flow with the layered structure remaining intact.^[126] Rakhi et al., demonstrated that Ti_2CT_x MXenes show a varied structure, composition, and properties by thermal treatment in air, Ar, N_2 , and N_2/H_2 mixture, respectively.^[118] Ti_2CT_x converts into numerous TiO_2 nanocrystals supported by ultrathin graphitic NSs after heat treatment in air, while the samples annealed in Ar, N_2 , and N_2/H_2 atmosphere retained the characteristic chemical structure and morphology. Particularly, the Ti_2CT_x sample after calcined in N_2/H_2 atmosphere exhibited significantly improved capacitive performance due to the elimination of surface F ions. Similarly, Thakur et al., systematically researched the stability of V_2CT_x MXenes in various environments (i.e., air, CO_2 , H_2 , and N_2) at temperatures up to 600 °C, as shown in Figure 10.^[128] V_2CT_x MXene materials transformed into V_2O_5 or a mixture of VO_x species above 300 °C in both air and CO_2 atmosphere with complete desertion of the initial layered structure, which could be maintained to a certain degree in a reducing environment (i.e., H_2). Meanwhile, the surface VO_x species could be reduced with surface terminals ($-\text{OH}$, $=\text{O}$, and $-\text{F}$) eliminated above 300 °C in an H_2 atmosphere. When the V_2CT_x compound was exposed to N_2 , the surface groups inevitably suffered from slight oxidation resulting from the reaction with intrinsic H_2O molecules contained in the as-fabricated MXenes. The layered structure remained intact up to 600 °C with the interlayer spacing decreased due to the dehydration of the material following the reaction:^[105]

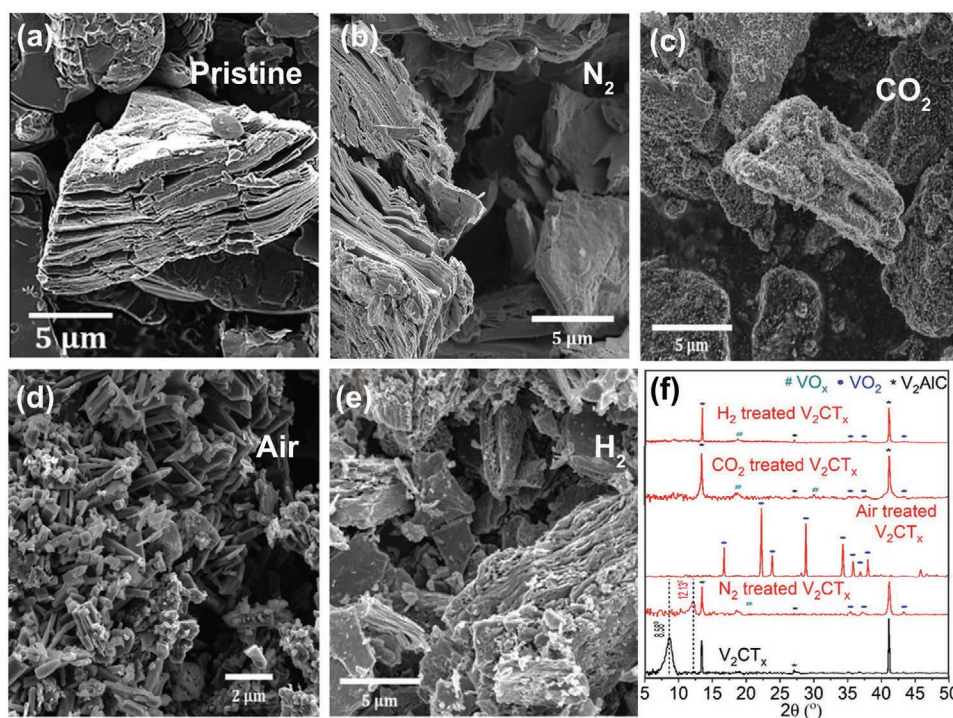
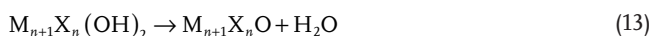


Figure 10. SEM images of a) V_2CT_x MXenes and V_2CT_x MXenes after heat treatment in b) N_2 , c) CO_2 , d) air, and e) H_2 at 600 °C with f) showing the corresponding XRD patterns. Reproduced with permission.^[128] Copyright 2019, The Royal Society of Chemistry.



Different atmospheres can be used for heat treatment, element-doping or in situ synthesis of MXene-derivatives with tunable oxidation degree. CO_2 , as a mild oxidant, is the most applied compound to partly oxidize MXenes to manufacture hierarchical structures.

4.2. Oxidation Temperature

The oxidation behavior of MXenes can be roughly classified into two different situations on account of the oxidation temperature. At lower temperatures, both the MXene phase and layered structure may be maintained. However, the oxidation activity becomes totally different at higher temperatures. The M layers are then oxidized as the center C layers completely disappear, and therefore the MXenes totally transform into a C/ TiO_2 composite with a well-ordered sandwich-type multilayer structure. The grain size and amount of TiO_2 tend to increase as the oxidation temperature increases, and the C layers, simultaneously, suffer oxidation resulting in a disintegrated structure. **Figure 11** presents SEM images and XRD patterns of Ti_3C_2 NSs after calcinations at various temperatures in vacuum. The initial structure of the 2D Ti_3C_2 MXenes can still retain at 600 °C (Figure 11a–c) with increased conductivity owing to its reduced surface groups and shortened conduction paths, which can offer a new possibility in the fabrication of high-quality MXenes with excellent performance.^[129] However, when further calcinated at 800 °C a collapse of the Ti_3C_2 NSs occurs with the formation of a large amount of rutile phase and a small quantity of anatase

TiO_2 (Figure 11e,f) as a result of oxidation reaction with the O_2 impurity in vacuum or with the =O/–OH groups terminated on the NS surface. Han et al., obtained different results for the calcination of $Ti_3C_2T_x$ MXenes at different temperatures in an Ar atmosphere.^[130] They found that the $Ti_3C_2T_x$ NSs retained the initial layered structures without visible TiO_2 or C phase morphology after annealing at 800 °C, but the disintegrated NSs annealed at 1000 °C.^[130] Xu et al., investigated the thermal stability of Ti_2CT_x by annealing from 500 to 800 °C in mixed gas of Ar and H_2 .^[131] The anatase TiO_2 emerged after annealing at 500 °C and then transferred into rutile TiO_2 after annealing at a higher temperature (e.g., 800 °C) without sacrificing the 2D multilayered structure. The TiO_2 NPs transformed into smaller ones, the surface became smooth and the interplane distances decreased with increasing annealing temperature. This structure evolution was found to strongly affect the dielectric properties of these compounds and their microwave absorbing performance. The initial layered structures can be maintained at a certain temperature. It is notable that the disintegration of the MXenes occurs at elevated temperatures even without an external oxidant supply in the system due to a combined effect of surface terminations and molecular hydrogen trapped between the MXene NSs. Therefore, it is important to control the surface terminations and molecular hydrogen trapped in the initial MXenes to improve the high temperature stability.

4.3. Humid and Aqueous Conditions

The durability of MXene solutions is of great significance because a lot of MXene-derived materials and devices are

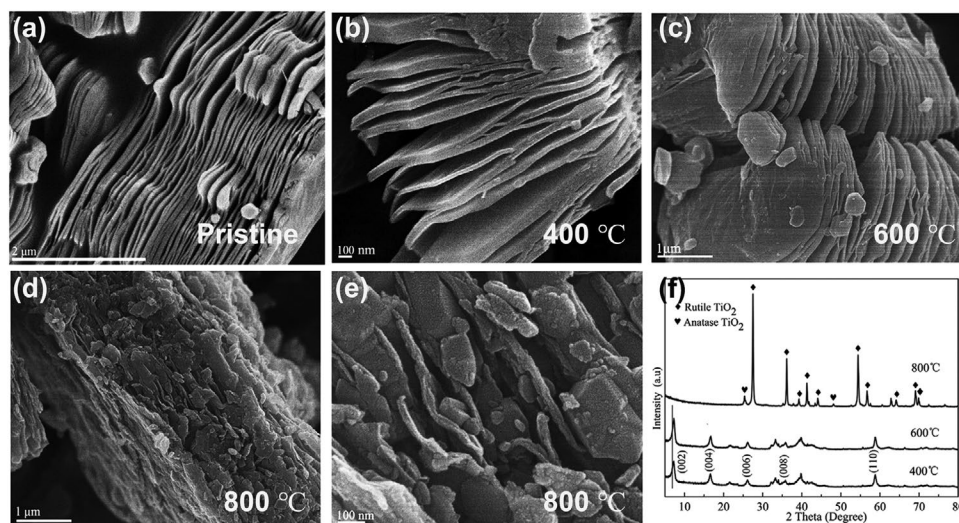
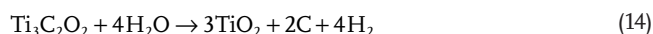


Figure 11. SEM images of a) MXene Ti_3C_2 NSs, MXene Ti_3C_2 NSs after calcination at b) 400 °C, c) 600 °C, d) 800 °C with e) high-magnification image of (d), and f) XRD patterns of MXene Ti_3C_2 NSs after calcinations at various temperatures. Reproduced with permission.^[129] Copyright 2015, Elsevier.

usually fabricated by utilizing such solutions.^[63] MXenes dispersed in aqueous solutions not only suffer from oxidation but also present a faster oxidation rate than that in freestanding MXenes.^[68,106] Besides, the oxidation mechanism of MXenes in an aqueous environment is quite complicated owing to the many potential parallel processes involved.^[65] Dissolved O_2 , aqueous environment, and higher temperatures may also seriously accelerate the degradation of MXene colloidal solutions, so more detailed studies are needed.^[63] Early reports have claimed that dissolved O_2 in water plays a significant part in the oxidation of MXene dispersions,^[63] while more recent studies have demonstrated that MXenes are more susceptible to reactions with H_2O molecules than dissolved O_2 .^[68,124,132] For example, the reaction between $\text{Ti}_3\text{C}_2\text{O}_2$ and H_2O :^[68,124,132]



The color changes of MXenes in different organic solvents can reflect how storage or dispersion media affect the oxidation processes. Maleski et al., found that the oxidation rate of $\text{Ti}_3\text{C}_2\text{T}_x$ in water was much faster than those in inorganic solvents, emphasizing the crucial participation of H_2O molecules in the $\text{Ti}_3\text{C}_2\text{T}_x$ oxidation process.^[133] It should be mentioned that color changes and colloidal stability are not consistent all the time. Thus, Habib et al., proposed conductivity measurements to assess the shelf life and oxidation process of $\text{Ti}_3\text{C}_2\text{T}_x$ in solids (e.g., ice and polymer), liquid (e.g., water and organic solvents), and air.^[68] The studies showed that $\text{Ti}_3\text{C}_2\text{T}_x$ proceeds oxidation degradation at the fastest speed in liquid solution, but the slowest rate in solid form.^[68] In terms of storage conditions, the preservation in ice or further freeze-drying to form a re-dispersible powder can decrease the oxidation of MXenes.

Apart from neutral solutions, other type solutions (e.g., alkaline or oxidizing solutions) have also attracted much research interest.^[134–137] Doo et al., proposed a different oxidation mechanism for aqueous Ti_3C_2 dispersions under various

pH conditions because the pH affects the formation of reaction intermediates between the $-\text{OH}$ terminal groups and H^+ or OH^- ions, as shown in Figure 9e.^[123] The protonated $-\text{OH}$ terminal groups on MXene NSs under acidic conditions make Ti atoms more electrophilic and susceptible to an oxidative nucleophilic addition reaction with H_2O or O_2 . As a result, the oxidative nucleophilic reaction of the MXene dispersion is accelerated under acidic conditions, whereas it is retarded under basic conditions as grounded on the exponential decay kinetics and activation energy. Conversely, Zhao et al., confirmed that the reaction with OH^- ions in basic media would accelerate the oxidation of MXenes according to the atomic percentage changes for the Ti(IV) component obtained by X-ray photoelectron spectroscopy.^[138] It was also demonstrated that the oxidation rate decreases when the MXene dispersion concentration is high due to a steric shielding effect among the nanosheets. Still, the mechanism of MXene degradation in aqueous environment has yet to be fully understood.

Cao et al., compared the oxidation process of Ti_3C_2 in water and sodium hydroxide (NaOH) solution at room temperature, see illustration in Figure 12.^[136] The results showed that TiO_2 NPs were primitively formed on the surface and interlayer of the Ti_3C_2 MXene NSs in aqueous solution. In contrast, TiO_2 nanowires were observed growing at the Ti_3C_2 MXene edges in an NaOH solution. The TiO_2 size and loading on the Ti_3C_2 surface increased with increasing reaction time or concentration of the NaOH solution. These two $\text{Ti}_3\text{C}_2/\text{TiO}_2$ hybrids showed excellent electrochemical performance when used as electrodes for supercapacitors.^[136] These findings are instructive and inspire more detailed investigations on controlling the morphology and quantity of the oxides that may directly instruct the production of high-performance devices. It has also been confirmed that MXenes show a faster oxidation rate in an H_2O_2 environment compared to wet and dry air environments.^[139] Ahmed et al., revealed that Ti_2C undergoes surface oxidation at room temperature when immersed in H_2O_2 solution, which can be described as below:^[134]

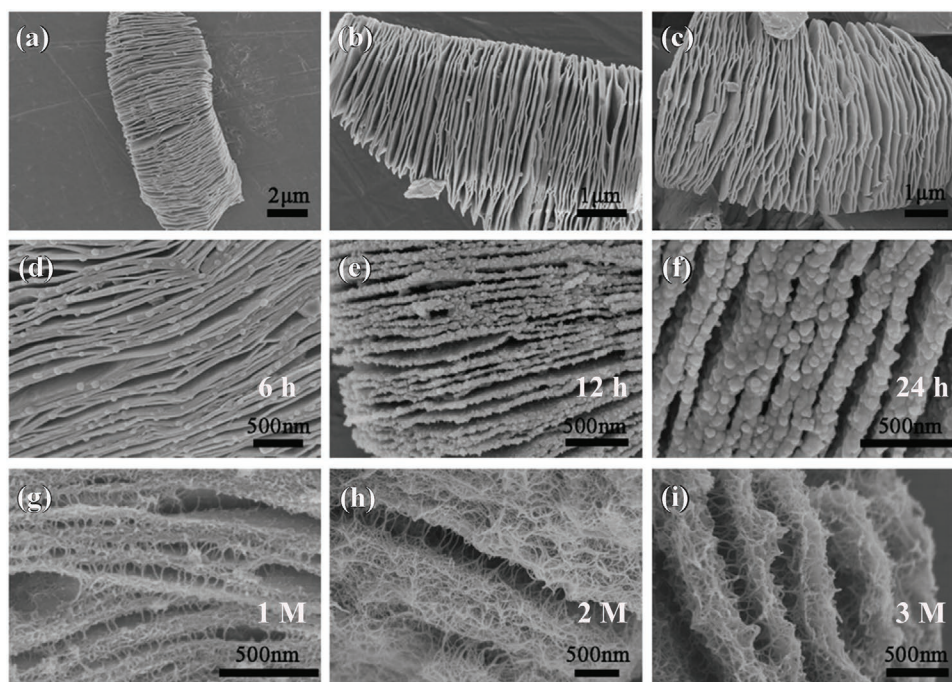
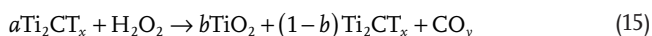


Figure 12. SEM images of a–c) Ti_3C_2 MXene, $\text{Ti}_3\text{C}_2/\text{TiO}_2$ -NPs obtained in water at room temperature for d) 6 h, e) 12 h, and f) 24 h, and $\text{Ti}_3\text{C}_2/\text{TiO}_2$ -nanowires formed in NaOH solution with the molar concentration of g) 1 M, h) 2 M, and i) 3 M at room temperature for 6 h. Reproduced with permission.^[136] Copyright 2017, ECS.



4.4. Intrinsic Chemical Composition and Structure of MXenes

The stability of MXenes greatly relies on their intrinsic chemical composition and microstructure, such as the types of M layers and the surface termination.^[140–142] Halim et al. investigated several types of MXenes (i.e., $\text{Ti}_3\text{C}_2\text{T}_x$, Ti_2CT_x , Ti_3CNT_x , Nb_2CT_x , and $\text{Nb}_4\text{C}_3\text{T}_x$), which displayed various degrees of oxidation with different amounts of oxidation products formed when exposed in air.^[143] According to the research conducted by Zhang et al., $\text{Nb}_4\text{C}_3\text{T}_x$ MXenes tend to oxidize in CO_2 atmosphere at 850 °C leading to a multilayer configuration with Nb_2O_5 NPs homogeneously formed on the MXene NSs surface.^[120] These results revealed that $\text{Nb}_4\text{C}_3\text{T}_x$ is less vulnerable to oxidation than $\text{Ti}_3\text{C}_2\text{T}_x$ that may suffer oxidation in CO_2 flow at a lower temperature (i.e., 500 °C). Zhou et al., studied the stability of both $\text{Zr}_3\text{C}_2\text{T}_x$ and $\text{Ti}_3\text{C}_2\text{T}_x$ at high temperature in both vacuum and argon atmosphere.^[141] Compared with Ti-based MXenes, $\text{Zr}_3\text{C}_2\text{T}_x$ possesses a comparatively better capability to retain 2D nature and structure integrity under same conditions.^[141] Similarly, Seredych et al., investigated the stability of $\text{Ti}_3\text{C}_2\text{T}_x$, Nb_2CT_x , and Mo_2CT_x up to 1500 °C under He atmosphere, respectively.^[100] $\text{Ti}_3\text{C}_2\text{T}_x$ could remain intact for processing temperatures within 800 °C that is much higher than the tolerated temperature of Nb_2CT_x and Mo_2CT_x , as shown in Figure 4. The incomplete oxidation and phase transformation of $\text{Ti}_3\text{C}_2\text{T}_x$ MXenes occurred beyond 850 °C. Therefore, $\text{Ti}_3\text{C}_2\text{T}_x$ is more thermally stable compared to few-atomic-layer Mo_2CT_x or Nb_2CT_x , and Mo_2CT_x exhibits less thermal stability

than Nb_2CT_x . This distinction in thermal stability at high temperatures can be explained in terms of the binding energy: The higher the binding energy, the better thermal stability of the MXenes. The binding energy (E_{binding}) can be defined as follows:^[141]

$$E_{\text{binding}} = \frac{\sum n_i E_{\text{atom}} - E_{\text{system}}}{\sum n_i} \quad (16)$$

where n_i is the atom number, E_{atom} is the energy of an isolated atom, and E_{system} is the total energy of the system. For example, the binding energy of $\text{Zr}_3\text{C}_2\text{T}_x$ is in this way estimated to be 8.483 eV, which is larger than the value for $\text{Ti}_3\text{C}_2\text{T}_x$ (8.080 eV). This is well consistent with the experimental results shown in Figure 13.^[141]

To date, a large number of studies on $\text{Ti}_3\text{C}_2\text{T}_x$ have been carried out. Most of the MXenes reported are carbides with few exceptions of nitrides and carbonitrides. While the investigation of new MXenes will certainly continue, systematic studies of the synthesis and properties of MXenes with different M, multi-M, X, and n is of great value for expanding the MXene community and advancing our understanding of these materials.

Knowing how the MXene surface is chemically terminated is also important for forecasting the characteristics and performance of materials. The molecule or atomic group chemisorbed on an MXene surface plays a crucial role in regulating the overall stoichiometry, stability, and characteristics owing to the generally high surface-to-volume ratio.^[14] The intrinsic H_2O molecules within the initial layered structure of MXenes might slightly oxidize the MXenes surface at high

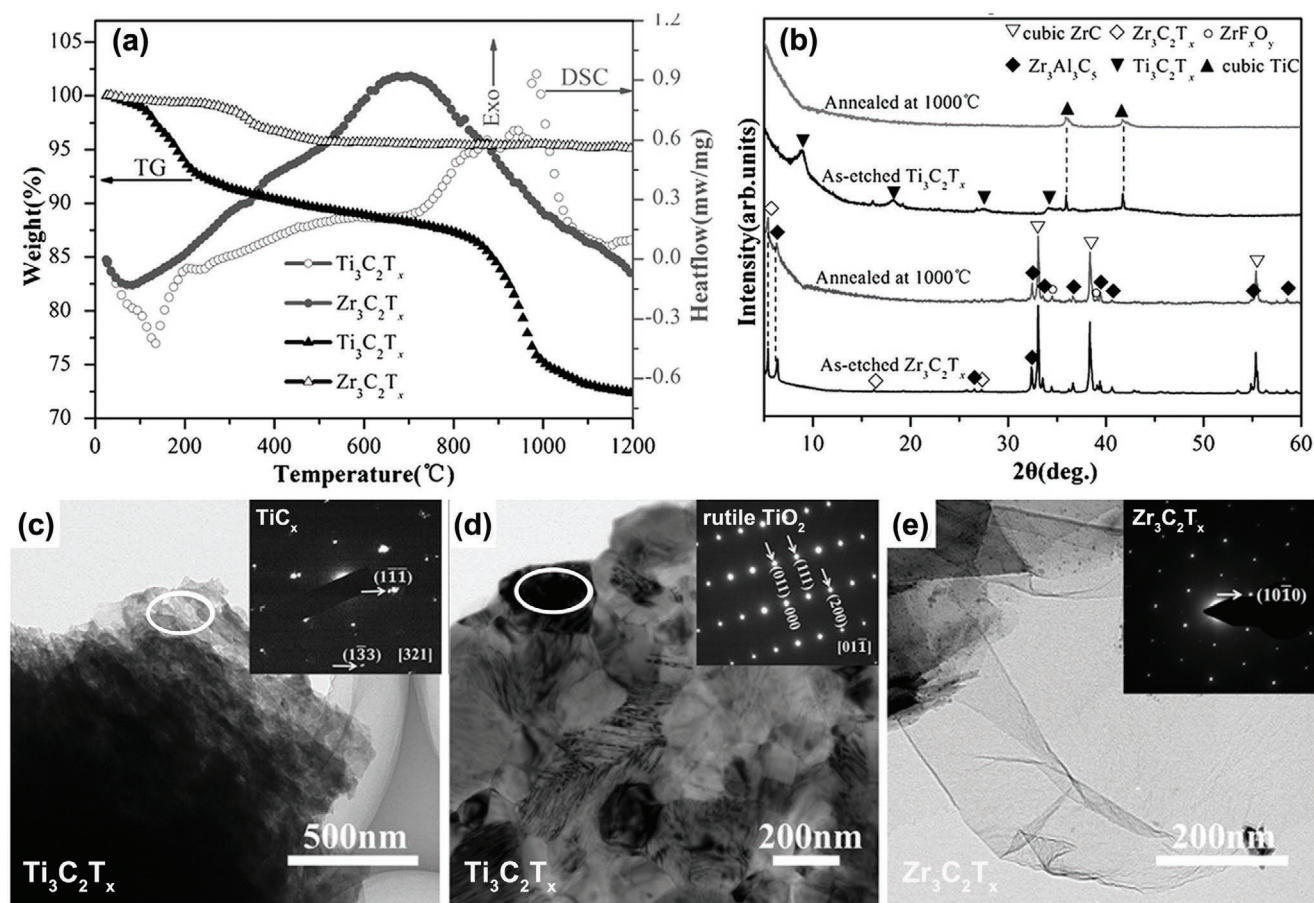


Figure 13. a,b) TG/DSC curves, c) XRD patterns, and d,e) TEM images with inset of SAED patterns of $\text{Ti}_3\text{C}_2\text{T}_x$ and $\text{Zr}_3\text{C}_2\text{T}_x$ before and after annealing in vacuum. Reproduced with permission.^[141] Copyright 2019, American Chemical Society.

temperatures regardless of atmosphere.^[128] Meanwhile, the surface terminations like =O and –OH that inevitably exist on an MXene surface after the topochemical deintercalations from MAX to MXene could simultaneously act as reactive forms of O_2 .^[5,31] These surface species could cause oxidation of the MXenes during heat treatment even without an external oxidant supply in the system.^[67,100] It has been demonstrated that the as-synthesized MXenes with –Cl terminations present better stability than the –F and =O terminated ones, which were thermally stable up to 750 °C.^[70,144] In this regard, the effects of more and novel surface terminations on the stability of MXenes still remain to be discovered and clarified, which would aid the design of MXenes with improved oxidation stability for a variety of future applications.

Recently, it has been recognized that the synthesis methods applied for high-quality MXenes with chemical and structural stability can be crucial for their different device applications in nanotechnology. However, HF etched multilayer MXene NSs usually show severe structural defects.^[80,100] Lipatov et al., revealed that the lower environmental stability of the $\text{Ti}_3\text{C}_2\text{T}_x$ NSs was caused by the presence of plenty of pin-hole defects, which usually promote the oxidation of MXene NSs in ambient environment.^[82] Ahmed et al., proposed that defects in MXenes could act as formation positions for metal oxide growth.^[134]

Xia et al., discovered that the oxidation of MXene NSs primarily happens near the defective sites that are generated by an internal electric field.^[119] The electron-hole buildup at Ti vacancies promotes the oxidation of C. The internal electric field formed by the buildup of electrons at NS ripples and edges results in Ti oxidation. The electric field further impels the development of the TiO_2 particles by promoting the migration of both Ti-cations and electrons, leading to the appearance of bigger voids and TiO_2 crystals.^[119] The mechanism for the establishment of an internal electric field is illustrated in **Figure 14**. These results could provide a new approach to alleviate oxidation through eliminating the generation of internal electric fields inherently produced nearby structural defects. However, the formation of structural defects (e.g., Ti vacancies, atomic steps, ripples, and holes) is inevitable during mechanical and chemical exfoliation processes.^[78]

Except for structural defects, degradation processes of MXene colloidal solutions shed light on the size-dependent stability of MXenes, for example, MXenes with smaller sizes are less stable.^[63] Therefore, the size optimization of MXene NSs in solutions has significant importance. The partition of MXene NSs of larger lateral size from smaller ones will not just prolong the storage time but also enhance the activity of the MXenes for different utilizations.

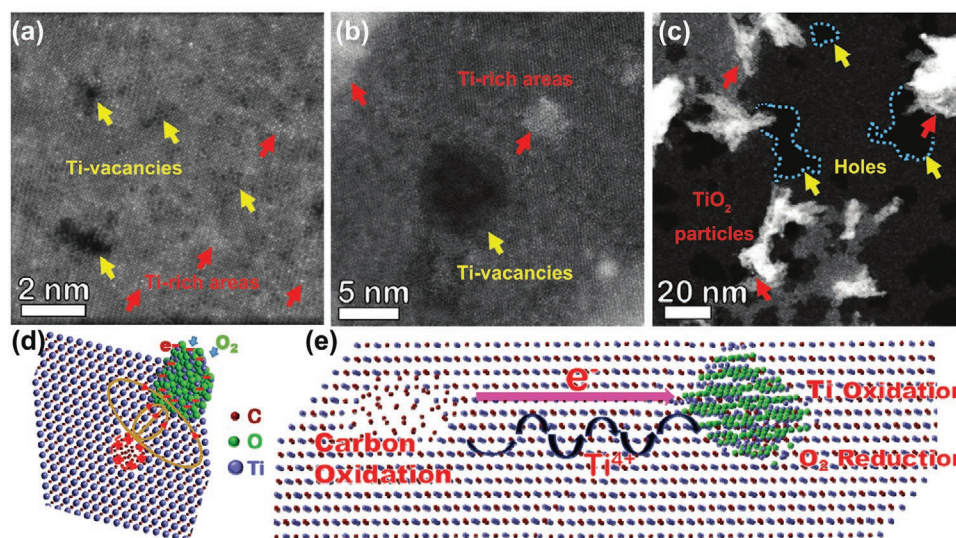


Figure 14. a,b) Z-contrast STEM images illustrating Ti-vacancies and Ti-rich areas, c) dark-field STEM images illustrating generation of TiO_2 particles with large holes nearby, d) schematic internal electric field, and e) Ti_2C_3 oxidation with C oxidized at the positive side and Ti oxidized at the negative side of the internal electric field. Reproduced with permission.^[119] Copyright 2019, The Royal Society of Chemistry.

5. Strategies to Mitigate Oxidation of MXenes

The instability of MXenes in air and water is a serious issue for their applications. Therefore, the urge to produce MXenes with good environmental stability or non-aqueous MXene devices has prompted imperative research on approaches to alleviate the oxidation and degradation of the MXenes.^[145] Several studies have been dedicated to reducing oxidation with well-controlled storage conditions or preparing MXenes completely isolated from water and O_2 .^[63,68,133,146,147] Oxidation can also be mitigated using antioxidants, for instance, polyphosphoric anions and ascorbates.^[148,149]

5.1. Preparation Optimization

It is generally believed that MXenes with fewer defects are chemically more stable because structural defect related sites are prone to promote oxidation nucleation as discussed in Section 4.4. Therefore, preparing high-quality MXenes with well-controlled defects is an efficient method to alter the oxidation kinetics and reduce the degree of oxidation.^[119] MXenes synthesized by employing mixed etchant acids (e.g., HCl/HF , LiF/HCl) or using bifluoride (e.g., NH_4HF_2) instead of only HF , present improved chemical stability as a consequence of the decreased defect concentration.^[100,150] Vahid Mohammadi et al., fabricated highly stable multilayered films of V_2CT_x by a cation-driven assembly process as illustrated in **Figure 15**, which relies on the electrostatic attraction between alkali-metal cations (AMs) and negatively charged MXene NSs to form ordered layered structures.^[121] The cation-driven assembly method can considerably suppress the oxidation of the V_2CT_x NSs, because the AM species (e.g., Li, Na, and Mg) are in a more reduced state in AM- V_2CT_x compared to delaminated V_2CT_x .^[151,152] The application of cation-driven assemblies is also available for other MXenes like Ti_2CT_x to fabricate

high-performance stable devices. Very recently, Mathis et al. proposed that Ti_3AlC_2 grains with improved structure and morphology can be produced by modifying the synthesis of Ti_3AlC_2 with excess Al ($\text{Al-Ti}_3\text{AlC}_2$).^[34] This feasible strategy can substantially improve the quality of the $\text{Al-Ti}_3\text{C}_2$ MXene NSs so obtained, and thereby significantly enhance the storage and chemical stability of the MXenes. As superior to conventional Ti_3C_2 , both an aqueous suspension and a freestanding film of $\text{Al-Ti}_3\text{C}_2$ exhibited a storage life more than 10 months with neglectable oxidation and only a slight degradation in properties, even in ambient conditions. The continuous development of synthesis optimization of MXenes, as well as, their MAX precursor is important for achieving new compositions and high quality of MXenes.

5.2. Heat Treatment

Oxidation reactions are expected to start from the functional group sites (e.g., $-\text{OH}$) that are the most vulnerable to the oxidation.^[119] Thermal annealing in vacuum or under inert atmosphere is an effective method to get rid of surface groups attached to MXenes and so to improve their intrinsic thermal stability for a wide range of applications.^[108,110,111,153] Wang et al., confirmed that bare MXenes (no surface terminations) obtained by heat treatment could remain intact at temperatures up to 1200 °C in Ar flow with merely a tiny amount of $\text{TiC}_x\text{O}_{1-x}$ ($0 < x < 1$) solid solution and some densification.^[80] Alternatively, Kamysbayev et al., introduced a strategy to tune or tailor surface terminations on MXenes by performing substitution or elimination reactions in molten inorganic salts.^[14] Heat treatment might potentially be used to heal nanoscale defects without causing harm to the characteristic multi-layer and hexagonal crystal structure of the MXenes. Lee et al., discovered that MXene films annealed in H_2 atmosphere oxidized at a reduced rate even under humid environment.^[106]

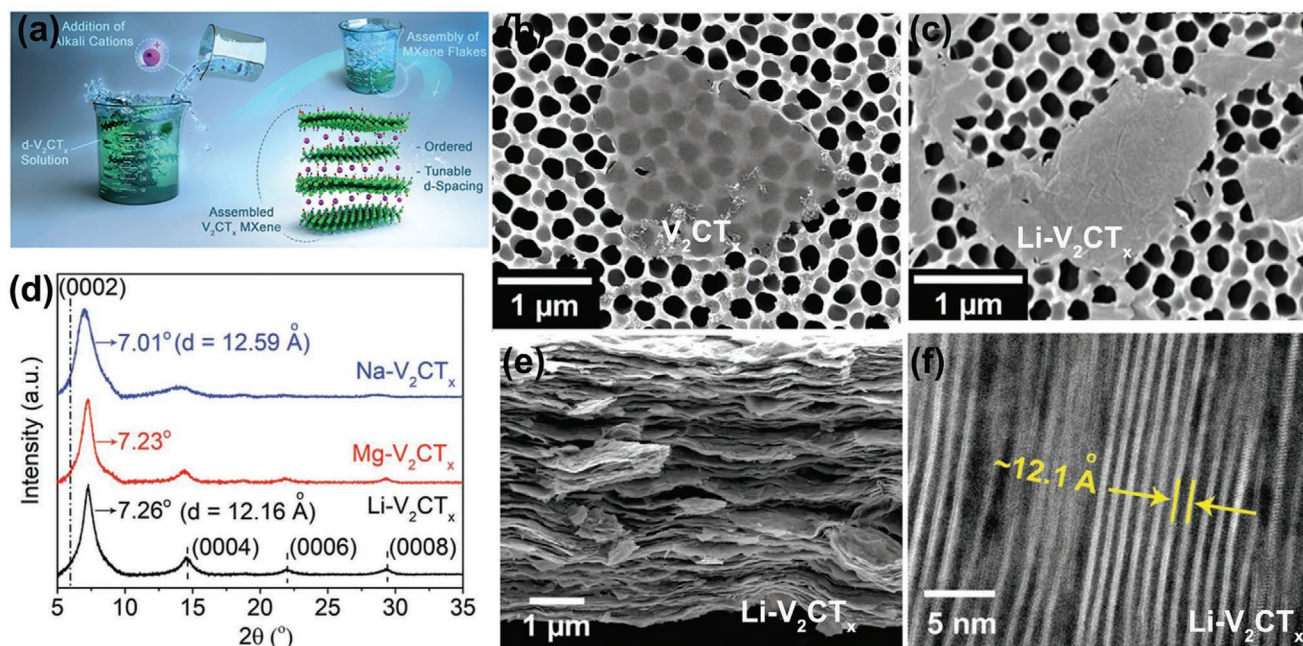


Figure 15. a) Schematic cation-driven assembly method for the preparation of V₂CT_x NSs with high stability, b,c) SEM images of single-layer V₂CT_x and Li-V₂CT_x. d) XRD patterns of films manufactured via NSs assembly with different cations, e) cross-sectional SEM image, and f) TEM image of layered structure Li-V₂CT_x film. Reproduced with permission.^[121] Copyright 2018, Wiley-VCH.

It is common knowledge that a well-developed and homogeneous surface encapsulation strategy can improve surface smoothness while also act as an extra barrier to ambient environment resulting in enhanced environmental stability of MXenes.^[146] Zhao et al., proved that developing a protective TiO₂ layer on an MXene film surface by thermal annealing

under inert Ar gas could significantly improve the stability.^[132] **Figure 16** shows a typical sandwich-structure film formed through an annealing process. The protective TiO₂ layer formed on films with more compact NSs stacking can prevent water penetration and deterioration of the internal configuration, which can significantly enhance the chemical stability of the

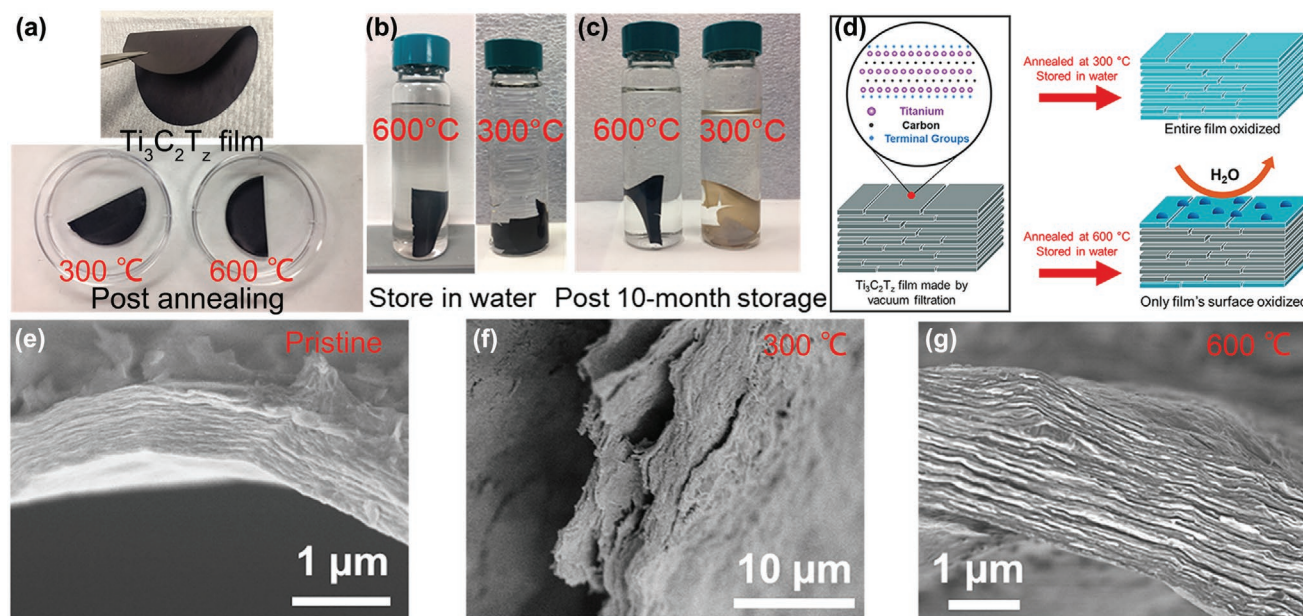


Figure 16. Images of a) Ti₃C₂ film, films annealed at 300 and 600 °C, annealed films stored in water after b) 24 h and c) 10 months. d) Diagram of Ti₃C₂ film annealed under argon, showing the oxidized layer on the films annealed at 600 °C acting as barriers to prevent water ingress and protect the inner layers. Cross-section SEM images of MXene films e) as-fabricated, annealed at f) 300 °C and g) 600 °C after stored in water for 10 months. Reproduced with permission.^[132] Copyright 2020, American Chemical Society.

surface with extended shelf life in an aqueous environment. Compared with an untreated $\text{Ti}_3\text{C}_2\text{T}_x$ film, the annealed $\text{Ti}_3\text{C}_2\text{T}_x$ films at 600 °C maintained stable in water for over 10 months, thereby endowing MXenes to exhibit more potential applications in a wide range of environments.^[132] In addition, the oxidation of high-quality $\text{Ti}_3\text{C}_2\text{T}_x$ NSs primitively occurs at the edges. It could therefore be a new feasible approach to alleviate oxidation via passivating edges using inert oxides or impermeable materials (e.g., hexagonal boron nitride).^[82,138,148]

5.3. Storage Conditions

Improvement of storage conditions is another important way to protect MXenes from oxidation. A lot of studies have indicated that the chemical stability can be greatly enhanced when the storage temperature is well controlled. Zhang et al., proposed an optimum environment to prolong the shelf time of MXene solutions by preparing concentrated NS solutions of large lateral size and storing in hermetic Ar-filled containers at cold environment (e.g., 5 °C).^[63] Stability could be considerably enhanced by storing in a deoxygenated atmosphere and refrigerating. Xia et al., found that MXenes stored in organic solvents without moisture presents enhanced stability. They discovered that the existence of water would benefit the local diffusion of Ti_4^+ and O_2^- ions involved during the oxidation process.^[119,147] Maleski et al., compared the stability of $\text{Ti}_3\text{C}_2\text{T}_x$ dispersions in 12 solvents, as shown in Figure 17.^[133] These results confirmed that $\text{Ti}_3\text{C}_2\text{T}_x$ dispersions in organic solvents (e.g., DMF, NMP, PC, and ethanol) can be an effective approach to alleviate or inhibit oxidation, thus extending the storage time of MXene colloidal solutions. These findings of stability in organic solvents simultaneously expand the opportunities for MXenes in a variety of processing techniques, such as the use of MXene–polymer composites and inks for 3D additive manufacturing.^[133] Besides, MXene powders can be separated from the colloidal solution via vacuum filtration or freeze-drying in order to completely avoid the undesired degradation caused by the aqueous environment.^[63] MXenes may also maintain their initial multilayer structure over a wide temperature range when protected under inert atmospheres like Ar, N_2 , and He.^[100,130]

Decreasing the amount of surface terminals (such as $-\text{OH}$) and intercalated water by hydrazine intercalation or TMs into MXenes can also enhance their stability.^[154,155] For example, Ling et al., evaluated the stability of TM- V_2CO_2 MXenes by ab initio molecular dynamics simulations.^[155] They found that there was no structure reconstruction in all of the cases under the temperature of 80 °C.^[155] The structures of the TM- V_2CO_2 still remained in good shape even after a temperature increase to 227 °C that far exceeded the typical experimental reaction temperature, indicating the high stability of TM- V_2CO_2 .^[155]

6. The Chemistry of MXene-Derived Oxides

As reviewed here, the inferior stability of MXene materials restricts their wide applications. Nevertheless, the family of MXenes has been proven to be a potential precursor for in situ synthesis of transition oxides/MXenes or transition oxides/carbon hybrid materials under proper oxidizing atmospheres and high temperature. Here, the MXenes not only serve as TM and C sources, but can also act as structure-directing agents. The products maintain the unique 2D layered structure of MXenes, meanwhile, transition oxides in situ grow on the layer surface. In particular, the partially or completely oxidized derivatives of Ti_3C_2 have been extensively studied.^[156]

6.1. Ti_3C_2 MXene Derived $\text{TiO}_2/\text{Ti}_3\text{C}_2$ Composites

Recently, Ti_3C_2 has been utilized as a potential platform for preparing TiO_2 via oxidation treatment owing to the feasibility of fabricating desired nanostructures. The Ti atoms in the Ti_3C_2 structure can serve as nucleation sites for the formation of TiO_2 , which directly encourages and promotes the homogeneous distribution in both size and structure. According to DFT, the Fermi level of Ti_3C_2 is nearly 0.18 eV versus NHE that is more positive compared to the conduction band (CB) of TiO_2 (−0.29 eV vs NHE).^[157] Therefore, it is constructive to form Schottky junctions between TiO_2 and Ti_3C_2 with the expectation to promote the migration of charge carriers. In such Schottky junction systems, electrons can migrate from CB of TiO_2 to Ti_3C_2 under light illumination, realizing the effective separation

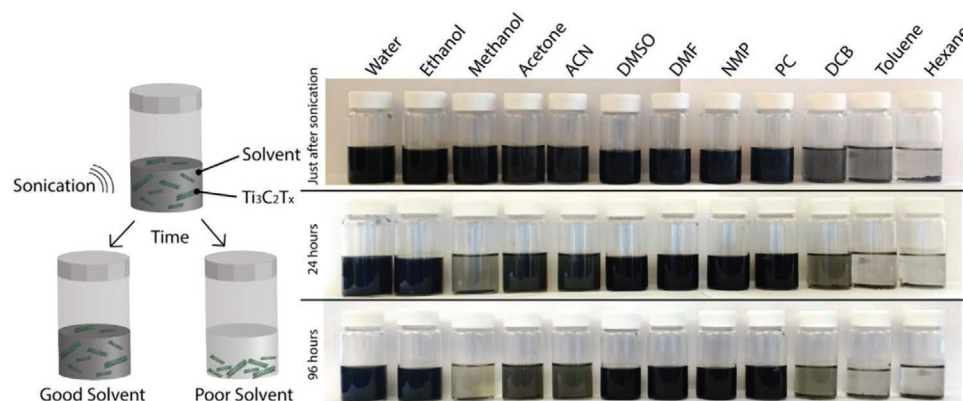


Figure 17. The stability of $\text{Ti}_3\text{C}_2\text{T}_x$ dispersions in 12 solvents via sonication after 0 h (top), 24 h (middle), and 96 h (bottom). Reproduced with permission.^[133] Copyright 2017, American Chemical Society.

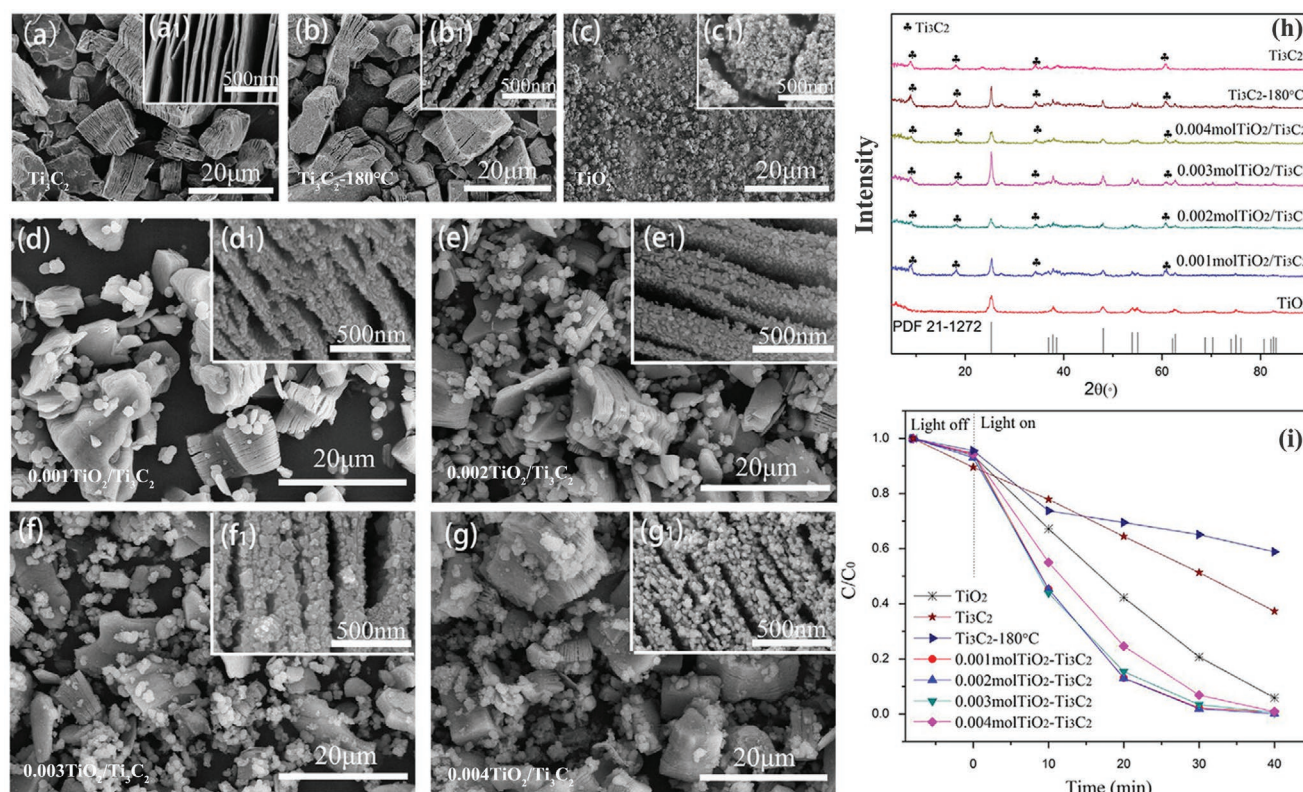


Figure 18. a–g) SEM images, h) XRD patterns, and i) the curves of photocatalytic degradation rate ($C_0/C-t$) of the as-prepared Ti_3C_2 , TiO_2 , and $\text{TiO}_2/\text{Ti}_3\text{C}_2$, respectively. Reproduced with permission.^[160] Copyright 2015, Elsevier.

of photogenerated electron/hole pairs.^[158] It is noticeable that the in situ development of homogeneous TiO_2 derived on Ti_3C_2 readily creates intimate interfacial contact with minimized defects, generating an atomic scale interfacial heterojunction.^[159] Consequently, the combination of both optically active TiO_2 and electrically conductive Ti_3C_2 shows unique higher charge carrier production, separation, and decreased recombination capability of photogenerated electrons, which attributes to the constructive Schottky structure formed at the $\text{TiO}_2/\text{Ti}_3\text{C}_2$ interface. Based on these favorable facts, the $\text{TiO}_2/\text{Ti}_3\text{C}_2$ composite can show stable and superior performance in the applications of dye degradation, CO_2 reduction, and sustainable hydrogen evolution reaction (HER).

As illustrated in **Figure 18**, Gao et al., prepared $\text{TiO}_2/\text{Ti}_3\text{C}_2$ nanocomposites with nanocrystals of anatase TiO_2 via a hydrothermal process, which showed better performance as photocatalyst for photodegradation of methyl orange under ultraviolet light illumination than did both pure TiO_2 and Ti_3C_2 MXenes.^[160] It was also confirmed that the in situ formation of TiO_2 on the MXene surfaces presented excellent performance of photocatalytic nitrogen fixation under full-spectrum irradiation.^[161,162] Notably, this nanocomposite showed good NH_3 selectivity with high electrochemical stability.^[161] Besides, the $\text{TiO}_2/\text{Ti}_3\text{C}_2$ delivered four times improvement in the photocatalytic HER than that of pristine rutile TiO_2 .^[163] Xu et al., suggested that the in situ obtained $\text{TiO}_2/\text{Ti}_3\text{C}_2$ heterostructure materials have great potential applications for efficient photoelectrocatalytic reduction of CO_2 to chemical fuels.^[164]

Moreover, Zhu et al., confirmed that $\text{TiO}_2/\text{Ti}_3\text{C}_2$ with high specific surface area guaranteed an ion diffusion process to occur between electrolyte and $\text{TiO}_2/\text{Ti}_3\text{C}_2$, which could increase specific capacitance, rate capacity, and stability. These results indicated promising use of $\text{TiO}_2/\text{Ti}_3\text{C}_2$ nanocomposites for supercapacitor energy storage.^[165] The Ti_3C_2 layers, however, tend to hinder the absorption of solar light and weaken the light intensity, resulting in reduced efficiency of solar light usage and photocatalytic activity. The inevitably overlapped layer structure of Ti_3C_2 NSs will not only decrease the electrical conductivity but also hinder the partition of electron/hole pairs. Additionally, the achieved electrochemical performance of the $\text{TiO}_2/\text{Ti}_3\text{C}_2$ composite is not sufficient for real applications on account of the inherent inferior electric conductivity and comparatively poor capacity of TiO_2 . The fabrication of $\text{TiO}_2/\text{Ti}_3\text{C}_2$ composites with a controllable content of TiO_2 and Ti_3C_2 is also a challenging issue. In general, electrical conductivity, active adsorption sites, $\text{TiO}_2/\text{Ti}_3\text{C}_2$ content ratio and uniform morphology and size are necessary factors to be further investigated and improved. To address these issues, a variety of strategies have been proposed and performed to enhance the properties of $\text{TiO}_2/\text{Ti}_3\text{C}_2$ composites.

6.1.1. Morphology Engineering Methods

During the in situ growth of $\text{TiO}_2/\text{Ti}_3\text{C}_2$ composites, many researchers have aimed to design various TiO_2 nanostructures

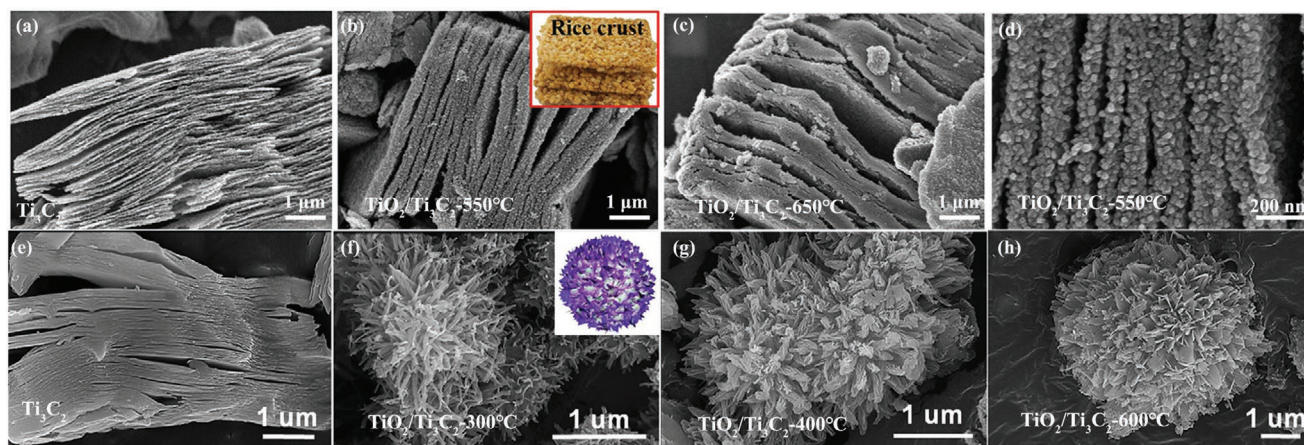


Figure 19. SEM images of Ti_3C_2 MXenes and $\text{TiO}_2/\text{Ti}_3\text{C}_2$ composites synthesized at different conditions: (a–d) rice crust morphology. Reproduced with permission.^[166] Copyright 2018, Elsevier; and (e–h) nanoflowers structure. Reproduced with permission.^[167] Copyright 2018, Elsevier.

at the interface of $\text{TiO}_2/\text{Ti}_3\text{C}_2$, including NSs, NPs, nanoflowers, nanowires etc., as shown in **Figure 19**. Low et al., fabricated a rice crust-like morphology with the homogeneous distribution of TiO_2 NPs on Ti_3C_2 by a calcination method.^[166] Li et al., successfully in situ manufactured $\text{TiO}_2/\text{Ti}_3\text{C}_2$ nanoflowers by a combination oxidation and alkalization process, and then applied ion exchange with post annealing procedures.^[167] These novel 3D structures could increase the specific surface regions, allow the sufficient exposure of reactive sites, improve light absorption, and shorten the photoexcited electron/hole migration distance. Morphology engineering can endow MXene high performance like superior capacity and long-term recycle stability even without additives of co-catalysts or sacrificial reagents.

6.1.2. Crystal Structure Modification

To obtain high performance, it has been suggested to expose the highly active facets and hybridizing with a suitable second phase in proper configurations. It has been demonstrated that in situ preparation of different orientational TiO_2 -MXene composites can be accomplished by tuning the growth of the crystallographic planes attributing to the existence of $-\text{F}$ species on the MXene surface.^[168] In particular, the development of specified crystal faces may be easily regulated during a solvothermal process by changing the solvents that interact with the $-\text{F}$ species on the MXene surface.^[169] As investigated earlier, the (001) facet of TiO_2 is more reactive than the (101) facet for photoexcitation.^[170] In this case, through the partial oxidation of Ti_3C_2 in a hydrothermal reaction, a heterojunction structure composed of layered Ti_3C_2 and TiO_2 with selectively exposure of the (001) facet could be achieved.^[171] Peng et al., designed a hybrid of 2D Ti_3C_2 and Ti^{3+} -doped rutile TiO_2 with the (111) facet exposed by using NH_4F as a facet controlling agent, in which the Ti^{3+} could self-dope into TiO_2 and narrow the band gap as shown in **Figure 20**.^[172] This special design takes the advantages of the facet effects, interfacial microstructure, and crystal vacancies, which can further enhance the activity of the $\text{TiO}_2/\text{Ti}_3\text{C}_2$ hybrids.^[172,173]

Moreover, the introduction of element modification has proved to be an efficient strategy to optimize the performance

of MXenes, as that can regulate the binding of the reactant or product species with catalysts, trim the electron-donor capability, improve the surface wettability and active sites of Ti_3C_2 .^[174] As illustrated in **Figure 21**, Ke et al., utilized diisopropyl amine (iPA) to produce N-doped Ti_3C_2 (iN- Ti_3C_2), which promoted electron transfer in Ti_3C_2 while inhibiting photo-generated electron/hole pair recombinations.^[175] The unique iN- $\text{Ti}_3\text{C}_2/\text{TiO}_2$ hybrid demonstrated excellent and consistent photocatalytic activity in the degradation of methylene blue, which is substantially more effective than pure TiO_2 , bulk- $\text{Ti}_3\text{C}_2/\text{TiO}_2$, and $\text{Ti}_3\text{C}_2/\text{TiO}_2$ hybrids. Meanwhile, the N-doped $\text{Ti}_3\text{C}_2/\text{TiO}_2$ hybrids are also promising anode materials, which display a high reversible capacity, long cycle lifetime and outstanding stability in Li-ion batteries.^[176] Similarly, MXenes adorned with phosphorus-doped TiO_2 (P- $\text{TiO}_2/\text{Ti}_3\text{C}_2$) showed improved electronic conduction, light absorption, activity and stability, opening up new possibilities for solar and electrical energy applications.^[177] Gao et al., investigated $\text{TiO}_2/\text{Ti}_3\text{C}_2$ heterojunction photocatalysts with Co modified by a two-step calcination method for photocatalytic nitrogen fixation.^[178] Co modification might change the chemisorption equilibrium of the catalyst for reactant (N_2) and product (NH_3), enhancing product desorption on the catalyst and increasing the active site efficiency, and resulting in a remarkable yield of ammonia in clean water.^[178]

Fabricating defect states that may affect the physicochemical characteristics like charge transport and optical property is another viable method for increasing MXene activity.^[177] For example, Miao et al. fabricated oxygen vacancy (OVs) modified $\text{TiO}_2/\text{Ti}_3\text{C}_2$ composites by using a hydrothermal oxidation method and heat treatment.^[158] It has also been demonstrated that adding OVs lowers the Schottky barrier and facilitates the transfer of photogenerated charge carriers, showing improved photocatalytic capability.^[158]

6.1.3. Heterojunction Nanostructure Constructions

Hybridizing $\text{TiO}_2/\text{Ti}_3\text{C}_2$ with additional active materials, for instance, MoS_2 , g- C_3N_4 , and graphene, into 3D architectures, is

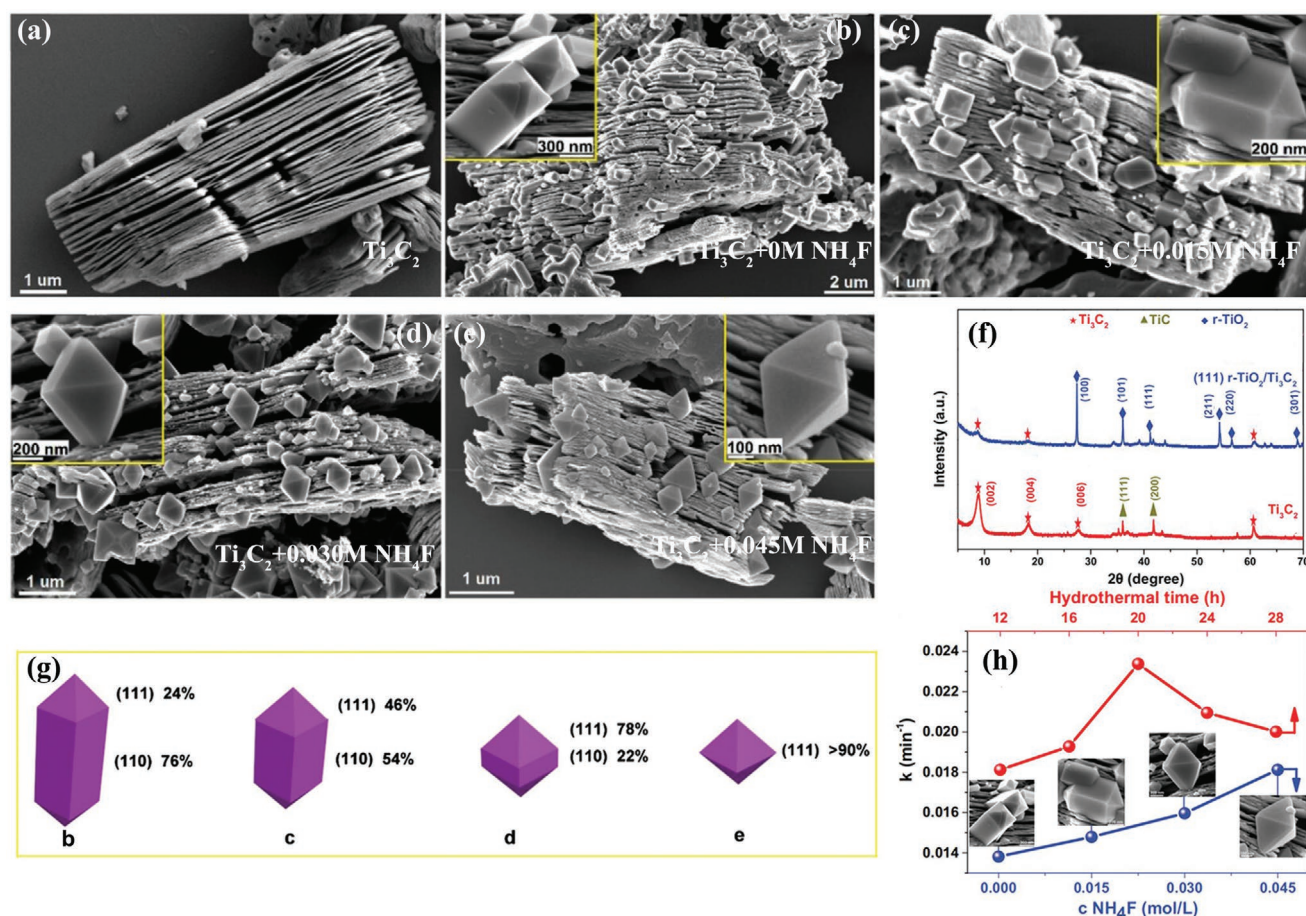


Figure 20. SEM images of a) Ti_3C_2 , and (111) $r\text{-TiO}_2/\text{Ti}_3\text{C}_2$ hybrids prepared with different content of NH_4F : b) 0 M, c) 0.015 M, d) 0.030 M, and e) 0.045 M, with g) showing the diagram of an individual TiO_2 particle in (b)–(e), f) XRD patterns of Ti_3C_2 and (111) $r\text{-TiO}_2/\text{Ti}_3\text{C}_2$, h) the correlation of the photocatalytic degradation rate of (111) $r\text{-TiO}_2/\text{Ti}_3\text{C}_2$ fabricated with concentrations of NH_4F and reaction time. Reproduced with permission.^[172] Copyright 2017, Elsevier.

another effective approach to enhance the properties of $\text{TiO}_2/\text{Ti}_3\text{C}_2$, because efficient charge separation can be achieved by coupling two semiconductor structures with matching energy levels.^[179–183] As a result, hierarchical $\text{TiO}_2/\text{Ti}_3\text{C}_2$ may be further used as an ideal platform and efficient co-catalyst to produce novel advanced materials. Li et al., reported a unique 2D based heterostructure of a $\text{Ti}_3\text{C}_2/\text{TiO}_2/\text{MoS}_2$ composite via a two-step hydrothermal process, in which TiO_2 NSs grew in situ on Ti_3C_2 MXenes with high-active (001) facets exposed and then MoS_2 NSs were deposited on the (101) facets of TiO_2 , as shown in Figure 22.^[180,181] The co-exposed (101) and (001) facets formed a surface heterostructure that endows a dual-carrier-separation mechanism, resulting in a notable improvement on activity and stability. Huang et al., performed a two-step hydrothermal oxidation to manufacture Ti_3C_2 MXenes embedded with TiO_2 NSs, which were further deposited with ZnIn_2S_4 (ZIS) to produce a new ternary 2D heterostructure of $\text{Ti}_3\text{C}_2/\text{TiO}_2/\text{ZIS}$.^[182] The hybrids with appropriate ZIS content showed a greater HER rate than $\text{Ti}_3\text{C}_2/\text{TiO}_2$ and pure ZIS, owing to the Schottky connection formed between ZIS and Ti_3C_2 . Hao et al., manufactured ternary NiFeCo -layered double hydroxide (LDH) NSs by in situ hybridization of Ti_3C_2 via a simple solvothermal method, and the incomplete oxidation of Ti_3C_2 simultaneously occurred

with anatase TiO_2 NPs being formed.^[183] While ternary LDH nanoplates and Ti_3C_2 NSs functioned as effective hole scavengers and shuttles for moving electrons and ions, respectively, the inclusion of TiO_2 NPs widened the light harvesting to enhance the formation of electron/hole pairs. Giving the synergistic effects between all of the components, these hybrid composites exhibit superior activity, such as, for the electrocatalytic oxygen evolution reaction.

6.2. Ti_3C_2 MXene Derived Carbon-Supported TiO_2

Theoretical and experimental studies have shown that MXene NSs provide a feasible platform for building unique configurations with isolated 2D C layers and TiO_2 NPs that serve as “bridges” to link the C layers.^[184] The 2D C layers act as electron migration conductors to promote charge separation efficiency, while the TiO_2 NPs provide electrons and holes under light excitation. Besides, the Ti_3C_2 -derived C layers have lower thickness than the pristine Ti_3C_2 NSs, which can effectively facilitate light harvesting without sacrificing light intensity.^[114] As a consequence, the 2D Ti_3C_2 -derived TiO_2/C hybrids possess many potential electrochemical characteristics, such as, increased

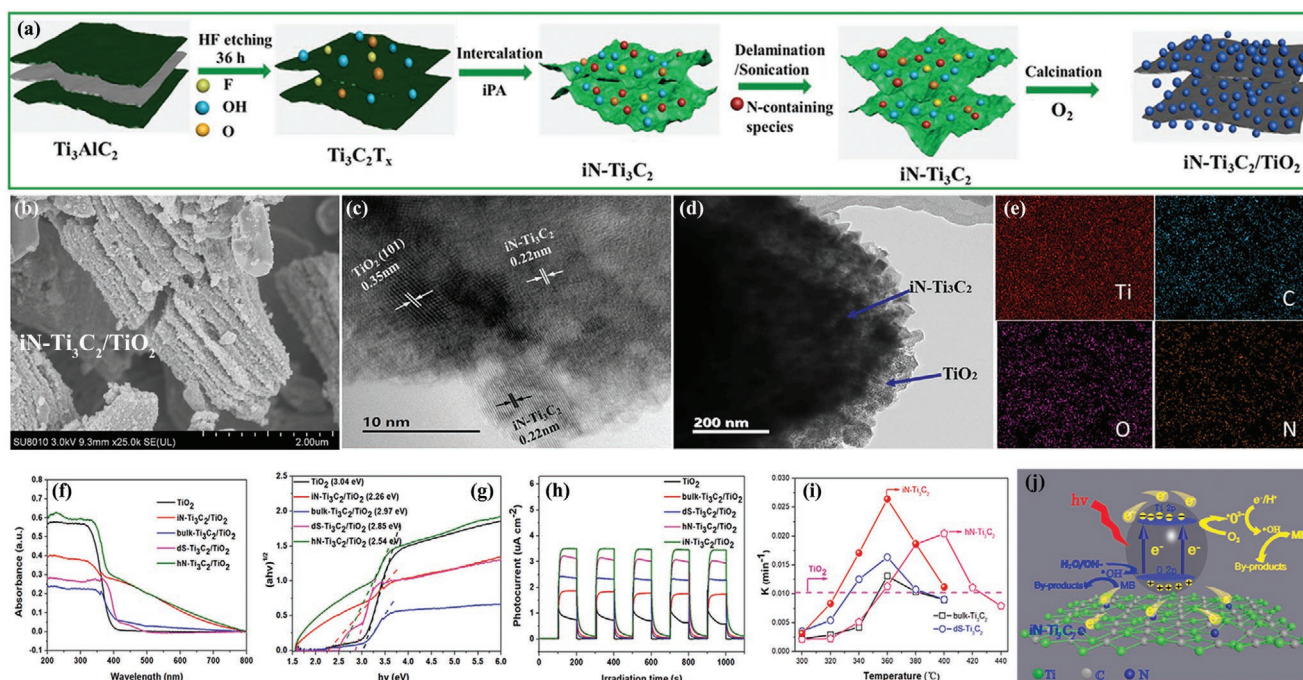


Figure 21. a) Diagram of in situ synthesis process, b) FESEM, c) TEM, d) HRTEM, e) EDS mapping of $iN-Ti_3C_2/TiO_2$. f) UV-vis diffuse reflectance spectra, g) Tauc-plots, h) transient photocurrent responses, i) the photocatalytic degradation rates of anatase TiO_2 and various optimized Ti_3C_2/TiO_2 . j) The proposed mechanism degradation of $iN-Ti_3C_2/TiO_2$ under ultraviolet light illumination. Reproduced with permission.^[175] Copyright 2020, Elsevier.

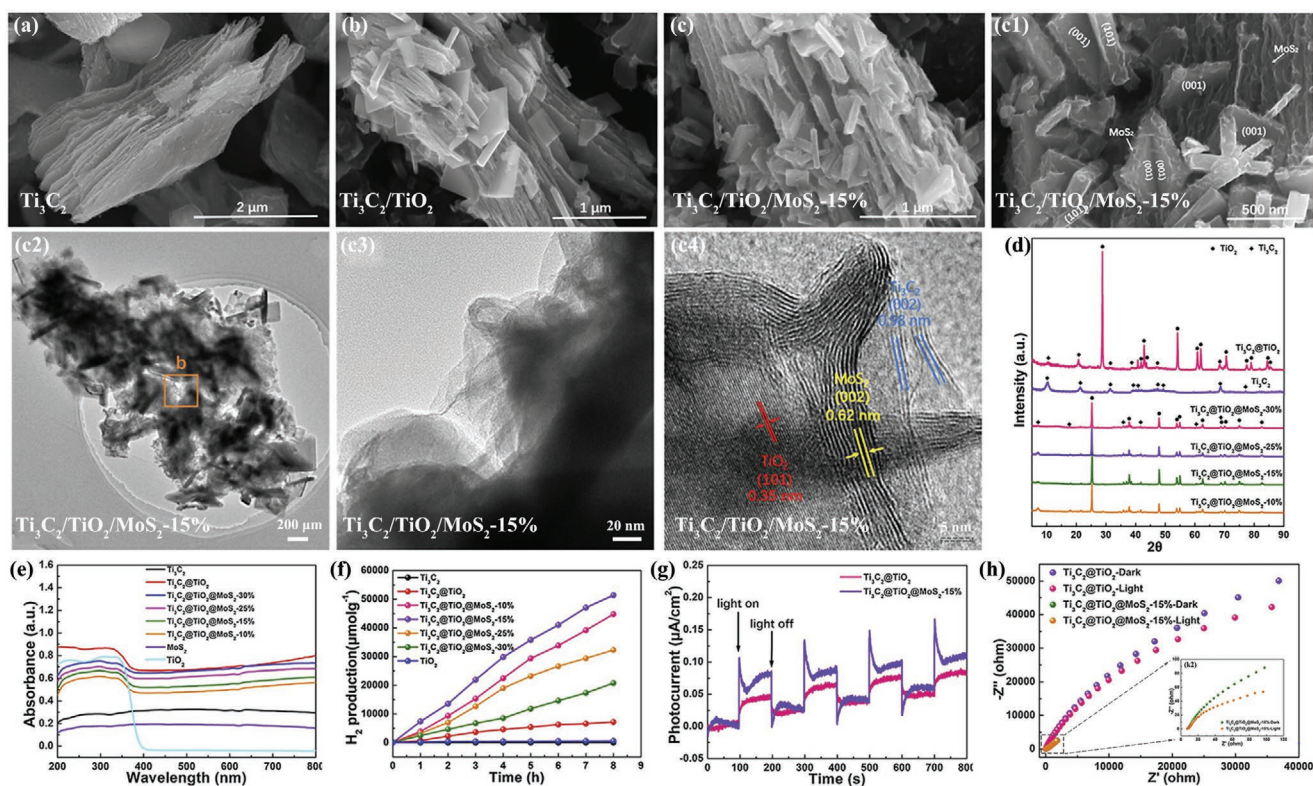


Figure 22. SEM images and TEM images of a) Ti_3C_2 , b) Ti_3C_2/TiO_2 hybrids, c) $Ti_3C_2/TiO_2/MoS_2-15\%$ hybrids. d) XRD patterns, e) UV-vis absorption spectra, f) photocatalytic HER, g) transient photocurrent response, and h) electrochemical impedance spectroscopy of Ti_3C_2 , Ti_3C_2/TiO_2 , $Ti_3C_2/TiO_2/MoS_2$ composites. Reproduced with permission.^[180] Copyright 2019, Elsevier.

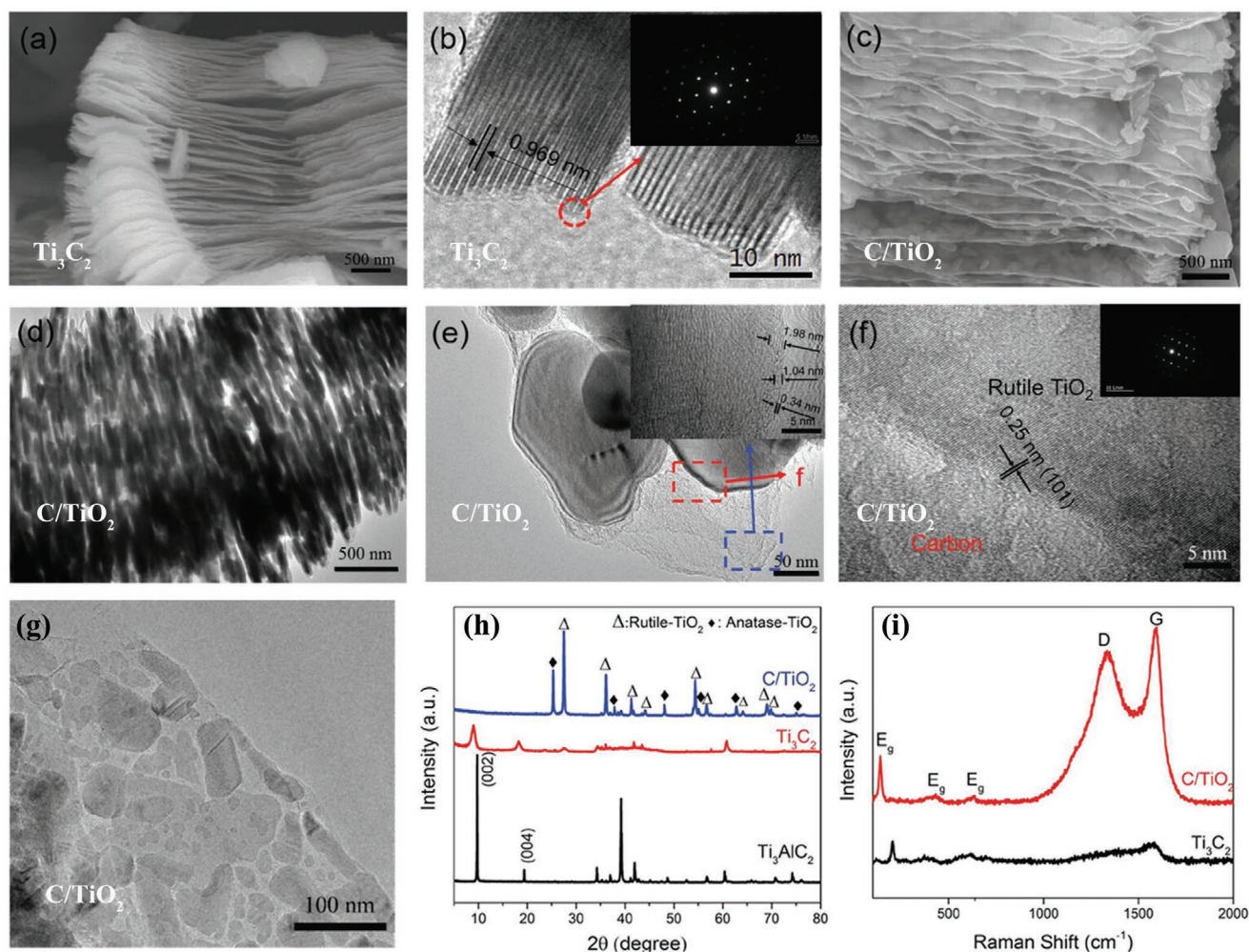


Figure 23. a,c) SEM images, b,d–g) TEM images, h) XRD patterns, i) Raman spectra of Ti_3C_2 and 2D C/TiO_2 composites, respectively, with inset in (b,f) showing the respective SAED images. Reproduced with permission.^[114] Copyright 2017, Wiley-VCH.

separation efficiency, high photocatalytic activity, and high light utilization. Naguib et al., discovered that TiO_2/C composites of layered structure can be obtained by oxidation transformation of Ti_3C_2 in CO_2 atmosphere or pressurized water.^[117] Zou et al., successfully fabricated urchin-like 2D TiO_2/C nanomaterials with a large number of (110) facets via an in situ solvothermal process with the participation of FeCl_3 solution.^[169] Recently, Yuan et al., proposed a facile one-step CO_2 oxidation process to manufacture 2D TiO_2/C hybrids from Ti_3C_2 , as illustrated in **Figure 23**.^[114]

The development of TiO_2 NPs on each NS greatly increases the specific surface area of the TiO_2/C composites. To achieve a high degree of crystallinity and well-preserved layered structure when transferring MXenes to their respective oxides, Tang et al., suggested a two-step oxidation procedure that incorporated pre-oxidation via a hydrothermal process followed by exposure in air at 300°C .^[135] Compared to directly oxidizing MXenes in air, the two-step oxidation method was able to reduce anomalous TiO_2 (a- TiO_2) grain growth while preserving the initial structure of the MXenes. However, how to control the uniformity of the structure and morphology of TiO_2 remains a tough issue. Ghassemi et al., performed an in situ TEM

investigation and discovered that TiO_2 NPs were primitively generated from the surface Ti layers in Ti_3C_2 under the flash oxidation.^[116] Considering that the pristine MXene NSs are often stacked together, it is challenging to form TiO_2/C composites with the layered structure that remained by completing oxidation of MXenes. Taking all of these aspects into account, a high-energy ball milling approach has been proposed to promote oxidation of Ti_2C MXenes to prepare TiO_2/C composites.^[185] Mechanical forces from ball milling readily destroy the van der Waals binding between the stacked Ti_2C , resulting in uniform and closely dispersed TiO_2 NPs on single or few-layered carbon NSs.

Furthermore, Huang et al., suggested to manufacture porous 2D layered N- TiO_2/C composites by calcinating Ti_3C_2 above 500°C with melamine and cetyltrimethyl ammonium bromide as N sources, as illustrated in **Figure 24a**.^[186] The N- TiO_2/C composites exhibit good stability, excellent conductivity, and increased photocatalytic performance, which present promising applications like wastewater treatment and air purification. Liang et al., achieved in situ preparation of N- TiO_2/C by a one-step hydrothermal reaction.^[188] Researchers have also tried strategic experimental approaches to produce TiO_2

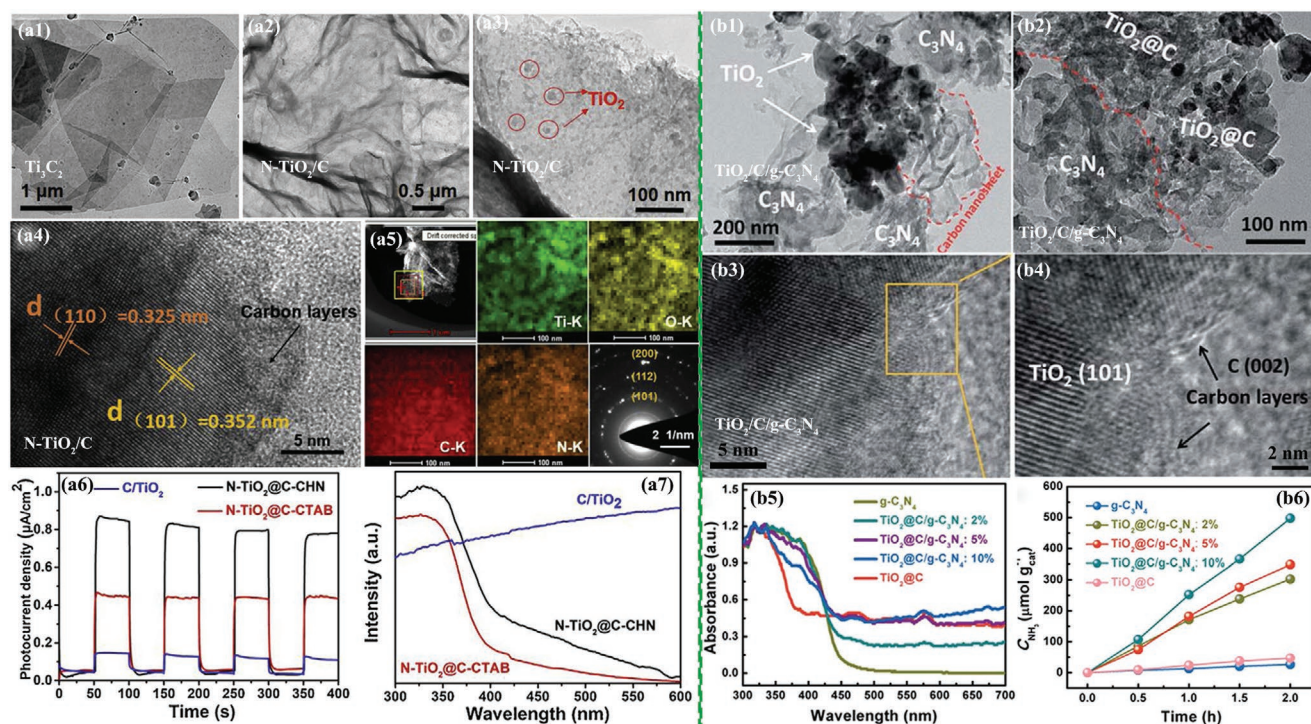


Figure 24. TEM images of a1) Ti₃C₂ MXene and a2–a4) N-TiO₂/C with a5) EDS mapping and SAED pattern of N-TiO₂/C. a6) The UV–vis absorption spectra and a7) the photocurrent density curves of the different N-TiO₂/C samples. Reproduced with permission.^[186] Copyright 2019, Elsevier. b1–b4) TEM images of TiO₂/C/g-C₃N₄ with b5) UV–vis diffuse reflectance absorption spectra and b6) photocatalytic activity of the systems of different TiO₂/C/g-C₃N₄ for NH₃ generation. Reproduced with permission.^[187] Copyright 2018, The Royal Society of Chemistry.

NPs efficiently contacted with in situ formed g-C₃N₄ NSs,^[187] or RGO, during the development of TiO₂/C composites.^[189] As demonstrated in Figure 24b, the TiO₂/C/g-C₃N₄ or TiO₂/RGO heterojunctions produced outstanding characteristics and enhanced functions. Furthermore, Zhang et al., proposed to construct a 3D TiO₂/N-doped C (NC)/Fe₇S₈ composite that combined the synergetic effects of TiO₂ with good structural stability, NC with excellent electrical conductivity and Fe₇S₈ with superior theoretical capacity.^[184] Similarly, Zhao et al., fabricated C layer supported amorphous TiO₂ NSs (a-TiO₂/C) coupled CdS via gamma-ray radiation-induced reduction and subsequent alkaline treatment for Ti₃C₂ MXenes at room temperature.^[190] These could be effective strategies for optimization on the basis of TiO₂/C composites to obtain advanced electrochemical performance and excellent cycling stability.

6.3. Hybrid Composites Derived from Nb-Based MXenes

Apart from the to date most widely studied Ti-based MXenes, other MXene-derived oxide hybrid composites have scarcely been reported. Recently, there has been raising concern about the oxidation of the new type of Nb-based MXenes. It has been reported that the additive of Nb₂C as co-catalyst endowed the TiO₂/Nb₂C composite better photocatalytic performance than TiO₂/Ti₃C₂ and TiO₂/Ti₂C.^[163] Meanwhile, Nb₂O₅ is a potential photocatalyst with good stability in chemical and photochemical properties, and has been applied for photocatalytic HER and degradation of organic pollutants.^[113] Therefore,

it can be hypothesized that an in situ development of Nb₂O₅ on Nb-based MXenes to produce Nb₂O₅/Nb₄C₃ hybrid nanostructures will provide fertile ground for potential applications in photocatalysis. Zhang et al., described a single-step oxidation process in CO₂ atmosphere at 850 °C for 0.5 h to create Nb₂O₅/Nb₄C₃ hierarchical composites.^[120] The hierarchical composite structure includes exterior formed crystalline Nb₂O₅ NPs that are linked to interior Nb₄C₃ layers via a C “bridge.” This special design takes all the advantages of Nb₂O₅ particles and conductive Nb₄C₃ layers, coupled with the effective electron “bridge” of C, which greatly enhances the performance of the Nb₂O₅/Nb₄C₃ hybrids. The approach utilizing CO₂ as a mild oxidant is also available to partly oxidize Nb₂C and Ti₃C₂ to manufacture similar hierarchical structures.^[120] In addition, the hierarchical Nb₂O₅/C/Nb₂C hybrid materials with amorphous C can also be achieved with well-controlled oxidation of Nb₂C in CO₂ flow, as shown in Figure 25.^[113,191] The optimized Nb₂O₅/C/Nb₂C composites exhibit more attractive electrochemical properties than Nb₂O₅ and mechanical Nb₂O₅/Nb₂C mixture in the same experimental conditions, attributing to the intimate junction between Nb₂O₅ and Nb₂C, together with the effective separation of photogenerated electron/hole pairs at the Nb₂O₅/Nb₂C interface. These preliminary results are encouraging and suggest that further work should be conducted for optimizing the volume fraction and particle size of the oxide particles to achieve better electrochemical performance. Besides, hierarchical composites obtained by this one-step oxidation in CO₂ mild oxidant is relatively simple and easily scalable, and can thus be applied for other MXene materials.

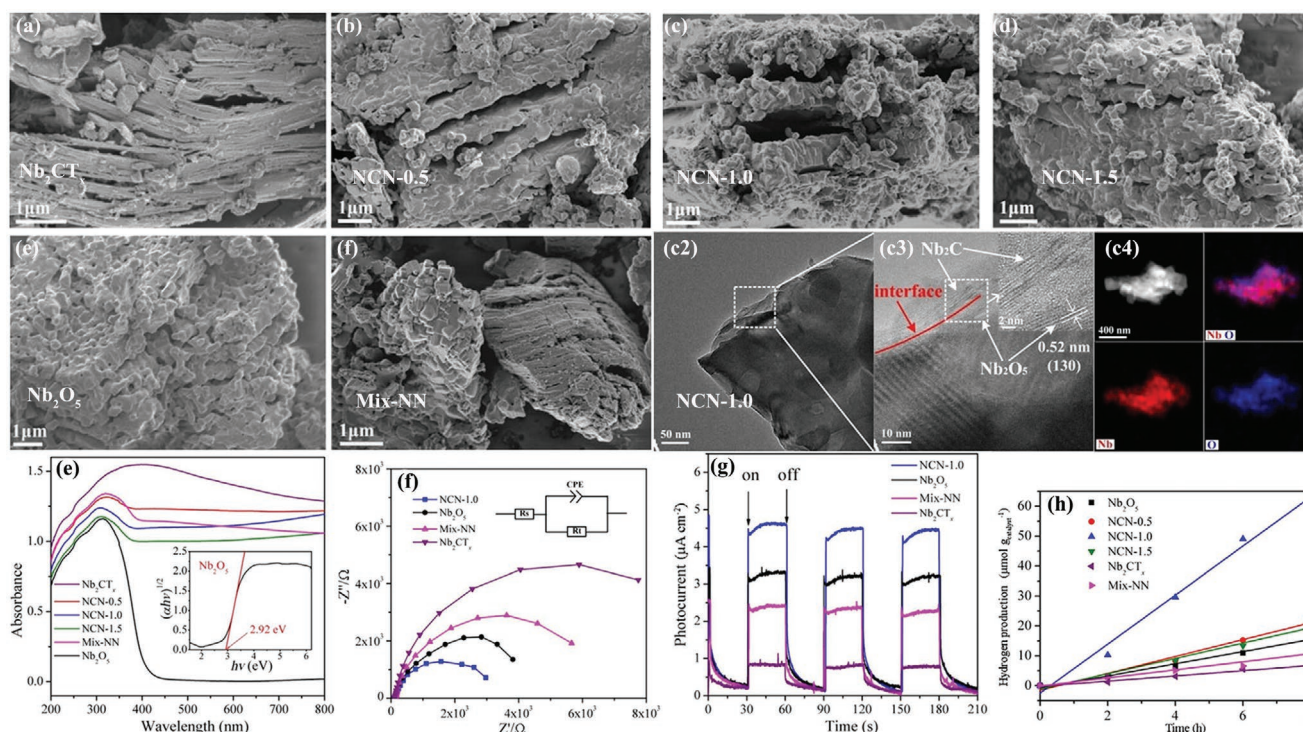


Figure 25. a–d) SEM images, TEM, HRTEM, and EDS analysis, e) UV–vis absorption spectra, f) Nyquist plots, g) photocurrents, h) time course of HER activity of Nb_2CT_x , $\text{Nb}_2\text{O}_5/\text{C}/\text{Nb}_2\text{C}$ oxidized for 0.5, 1.0, or 1.5 h (NCN-0.5, NCN-1.0, NCN-1.5), Nb_2O_5 , and a mechanically mixed $\text{Nb}_2\text{O}_5/\text{Nb}_2\text{C}$ sample (Mix-NN). Reproduced with permission.^[113] Copyright 2018, Wiley-VCH.

7. Conclusion and Perspective

MXenes possess exclusive morphologies, mechanical and electronic performance, which have triggered an ever-increasing attention to the development of MXenes for a range of applications. It has though been realized that the environmental instability is a serious challenge for processing and commercial utilization of MXene-based devices. MXenes can readily degrade into collapsed structures and decorated with oxides as a result of the combined effects from air, moisture, and light. The degradation processes can severely destroy the structural integrity and affect the activity of the MXenes.

The structural and chemical stability of MXenes is extremely susceptible to an oxidizing atmosphere (air, O_2 , CO_2 , etc.) and high temperature. The stability of MXenes greatly relies on their intrinsic chemical composition and microstructure, such as, the type of surface termination and M layers. Structural variations of MXenes occur at elevated temperatures even without an external oxidant supply in the system often due to a combination of surface terminations and molecular hydrogen trapped between the MXene NSs. Oxidation reactions are expected to start from the functional group sites (e.g., $-\text{OH}$) that are most vulnerable to the oxidation. Thermal annealing in vacuum or under inert atmosphere is an effective method to get rid of surface groups attached to MXenes and so to improve their intrinsic thermal stability. Heat treatment might simultaneously induce crystal structure variation, such as interlayer spacing reduction, defect healing and twinning transformation. Besides, the $-\text{Cl}$ terminated synthesized MXenes present better stability than the $-\text{F}$ and $=\text{O}$ terminated ones,

and there are still new termination systems that remain to be identified with potential opportunity to prepare MXenes with improved performance. Tuning or tailoring surface terminations (e.g., $\text{T} = \text{S}$, Cl , Se , Br , Te) on MXenes can be achieved by performing substitution or elimination reactions in different compositions of molten inorganic salts, such as Lewis acid and Lewis-base molten salts.

To date, numerous MXenes have been synthesized, but most of the MXenes reported are carbides with some exceptions of nitrides and carbonitrides, in which only a few types of MXenes have attracted experimental investigations on their oxidation performance (e.g., $\text{Ti}_3\text{C}_2\text{T}_x$ and Nb_2CT_x). The distinction in stability of different MXenes is still not well understood in spite of predictions in terms of binding energy based on theoretical calculations. It is necessary to explore preferable and promising MXenes (like $\text{Nb}_4\text{C}_3\text{T}_x$, $\text{Zr}_3\text{C}_2\text{T}_x$) for the applications in severe environments, especially when serving at a relatively high temperature. Systematic studies of the synthesis and properties of MXenes with different M, multi-M, X, and n is of a great value for expanding the MXenes community and advancing our understanding of their intrinsic stability.

The oxidation of MXene NSs primitively happens near the defective sites. The influence mechanism of structure defects (e.g., Ti vacancies, atomic steps, ripples and holes) on MXene oxidation is very complicated involving internal electric fields inherently produced, which promotes the migration of both Ti-cations and electrons, leading to the appearance of bigger voids and TiO_2 crystals. Oxidation can thus be alleviated through eliminating the generation of internal electric fields inherently produced nearby structural defects. However, the

structural defects are inevitable during mechanical and chemical exfoliation processes. Environmentally friendly, safe, efficient, and scalable synthesis methods, for example by using a mixed lithium fluoride-hydrochloric acid (LiF-HCl), or bismuth fluoride (e.g., NH_4HF_2 , NaHF_2 , and KHF_2) etching solution instead of immersing in concentrated HF solution, can achieve desired MXene NSs with large lateral size and fewer defects. Instead of being in wet chemical environments, MXenes obtained by CVD often exhibit large size, high crystallinity, and defect-free structure with no terminations, which provides possibilities for the investigation on the intrinsic properties of the MXenes. However, the cost and strict conditions of the CVD process of MXene preparation are challenging issues in order to achieve wider applications.

The durability of MXene solutions is of great significance because a lot of MXene-derived materials and devices are usually fabricated by utilizing such solutions. MXenes dispersed in aqueous solutions not only suffer from oxidation but also present a faster oxidation rate than that in the freestanding MXenes. Besides, the oxidation mechanism of MXenes in an aqueous environment is quite complicated owing to the many potential parallel processes involved. Thus the mechanism of MXene degradation in aqueous environment has yet to be fully understood. A well-developed and homogeneous surface encapsulation strategy can improve surface smoothness while also act as an extra barrier to ambient environments resulting in enhanced environmental stability of the MXenes. Considering that the oxidation of MXene NSs primitively occurs at the edges, the oxidation can be alleviated via passivating the edges using inert oxides or impermeable materials. The size optimization of MXene NSs in solutions has also a significant importance. The partition of MXene NSs of larger lateral size from smaller ones will not just prolong the storage time but also enhance the activity of MXenes for different utilizations. Improvement of storage conditions in a deoxygenated atmosphere and refrigerating environment is another important way to protect MXenes from oxidation. Stability can also be considerably enhanced by storing in organic solvents without moisture because the existence of water benefits the local diffusion of Ti_4^+ and O_2^- ions involved during the oxidation process. These findings of MXene stability in organic solvents simultaneously expand the opportunities for MXenes in a variety of processing techniques, such as using MXene-polymer composites and inks for 3D additive manufacturing. Besides, MXene powders can be separated from the colloidal solution via vacuum filtration or freeze-drying in order to completely avoid the undesired degradation caused by the aqueous environment. MXenes may also maintain their initial multilayer structure over a wide temperature range when protected under inert atmospheres like Ar, N_2 , and He.

In general, modified synthesis methods and subsequent treatment or storage technologies for obtaining high-quality MXenes with well-controlled surface functional groups, large lateral size and few defects, as well as, their precursor MAX phase, constitute effective ways to improve the intrinsic thermal stability.

The degradation temperature of MXenes strongly depends on their chemical composition and initial structure, but the structural variation of different MXenes follows a general rule: From MXenes to MXene/oxide NSs, C/oxide NSs, and final

oxide products. This has significantly inspired the in situ synthesis of novel architectures of nanohybrid structures under well-controlled oxidation processes with the unique 2D layered structure of the MXenes retained. These findings are instructive and indicate that more detailed investigations on controlling the morphology and quantity of the MXene-derivatives may directly instruct the production of high-performance devices. Desired phase composition and morphology of MXene-derivatives can be achieved by manipulating the oxidation atmosphere, temperature and oxidation rate. Thus, it is especially imperative to explore and understand the oxidation kinetics of MXenes for predicting their composition and performance with the passage of time. It has been reported that oxidation of Ti_3C_2 MXenes follows a single exponential decay behavior. More detailed research should be performed to reveal the applicability of the exponential decay for other MXene materials.

MXene-derived composites with the intimate constructive Schottky structure exhibit advanced electrochemical performance and excellent cycling stability for promising applications in a broad range of environments, which present perspectives for the challenges and opportunities of the oxidation chemistry of MXenes and bring new research significance to their protection and application. Based on the most widely studied Ti-based MXenes to date, the obtained electrochemical activity is not sufficient for practical applications because of the inherent poor electrical conductivity and comparatively low capacity of TiO_2 . Various strategies in terms of morphology engineering, crystal structure modification, and heterojunction nanostructure construction are required to be performed in order to improve the conductivity, the active adsorption sites, and the uniformity of morphology and size with well-controlled TiO_2 content of MXene-derived composites to obtain superior physico-chemical performance. These preliminary results are encouraging and suggest further research to unravel the oxidation chemistry and applications of MXenes in general but also for novel and complicated MXenes such as high-entropy MXenes like TiVN-bMoC_3 and TiVCrMoC_3 .

Acknowledgements

This work was supported by the National Natural Science Foundation of China (No. 12005094, 61905157), the Natural Science Foundation of Hunan Province (No. 2020JJ5485), Fund of University of South China (Grant No. 201RGC009), and National Postdoctoral Program for Innovative Talents (BX20190236).

Conflict of Interest

The authors declare no conflict of interest.

Keywords

2D, applications, MXenes, oxidation, stability

Received: September 22, 2021

Revised: November 10, 2021

Published online: February 17, 2022

- [1] M. Naguib, M. Kurtoglu, V. Presser, J. Lu, J. Niu, M. Heon, L. Hultman, Y. Gogotsi, M. Barsoum, *Adv. Mater.* **2011**, 23, 4248.
- [2] M. Barsoum, *Prog. Solid St. Chem.* **2000**, 28, 201.
- [3] M. Magnuson, M. Mattesini, *Thin Solid Films* **2017**, 621, 108.
- [4] M. Radovic, M. Barsoum, *Am. Ceram. Soc. Bull.* **2013**, 92, 20.
- [5] M. Naguib, Y. Gogotsi, *Acc. Chem. Res.* **2015**, 48, 128.
- [6] M. Alhabeb, K. Maleski, T. Mathis, A. Sarycheva, C. Hatter, S. Uzun, A. Levitt, Y. Gogotsi, *Angew. Chem., Int. Ed.* **2018**, 57, 5444.
- [7] P. Srivastava, A. Mishra, H. Mizuseki, K. Lee, A. Singh, *ACS Appl. Mater. Interfaces* **2016**, 8, 24256.
- [8] M. Alhabeb, K. Maleski, B. Anasori, P. Lelyukh, L. Clark, S. Sin, Y. Gogotsi, *Chem. Mater.* **2017**, 29, 7633.
- [9] L. Karlsson, J. Birch, J. Halim, M. Barsoum, P. Persson, *Nano Lett.* **2015**, 15, 4955.
- [10] M. Naguib, V. Mochalin, M. Barsoum, Y. Gogotsi, *Adv. Mater.* **2014**, 26, 992.
- [11] Y. Gogotsi, B. Anasori, *ACS Nano* **2019**, 13, 8491.
- [12] H. Zhang, *ACS Nano* **2015**, 9, 9451.
- [13] K. Maleski, C. Shuck, A. Fafarman, Y. Gogotsi, *Adv. Opt. Mater.* **2020**, 9, 2001563.
- [14] V. Kamsybayev, A. Filatov, H. Hu, X. Rui, F. Lagunas, D. Wang, R. Klie, D. Talapin, *Science* **2020**, 369, 979.
- [15] H. Pazniak, M. Benchakar, T. Bilyk, A. Liedl, Y. Busby, C. Noel, P. Chartier, S. Hurand, M. Marteau, L. Houssiau, R. Larciprete, P. Lacovig, D. Lizzit, E. Tosi, S. Lizzit, J. Pacaud, S. Celerier, V. Mauchamp, M. David, *ACS Nano* **2021**, 15, 4245.
- [16] S. Lai, J. Jeon, S. Jang, J. Xu, Y. Choi, J. Park, E. Hwang, S. Lee, *Nanoscale* **2015**, 7, 19390.
- [17] J. Xuan, Z. Wang, Y. Chen, D. Liang, L. Cheng, X. Yang, Z. Liu, R. Ma, T. Sasaki, F. Geng, *Angew. Chem., Int. Ed.* **2016**, 55, 14569.
- [18] J. Li, X. Yuan, C. Lin, Y. Yang, L. Xu, X. Du, J. Xie, J. Lin, J. Sun, *Adv. Energy Mater.* **2017**, 7, 1602725.
- [19] S. Li, P. Tuo, J. Xie, X. Zhang, J. Xu, J. Bao, B. Pan, Y. Xie, *Nano Energy* **2018**, 47, 512.
- [20] X. Chen, Z. Kong, N. Li, X. Zhao, C. Sun, *Phys. Chem. Chem. Phys.* **2016**, 18, 32937.
- [21] H. Oschinski, A. Morales-Garcia, F. Illas, *J. Phys. Chem. C* **2021**, 125, 2477.
- [22] A. Mostafaei, M. Abbasnejad, *J. Alloys Compd.* **2021**, 857, 157982.
- [23] J. Thornberg, J. Halim, J. Lu, R. Meshkian, J. Palisaitis, L. Hultman, P. Persson, J. Rosen, *Nanoscale* **2019**, 11, 14720.
- [24] A. Enyashin, A. Ivanovskii, *J. Solid State Chem.* **2013**, 207, 42.
- [25] B. Anasori, Y. Xie, M. Beidaghi, J. Lu, B. Hosler, L. Hultman, P. Kent, Y. Gogotsi, M. Barsoum, *ACS Nano* **2015**, 9, 9507.
- [26] J. Yang, G. Yao, S. Sun, Z. Chen, S. Yuan, K. Wu, X. Fu, Q. Wang, W. Cui, *Carbon* **2021**, 179, 104.
- [27] S. Neman, B. Zhang, B. Wyatt, Z. Hood, S. Manna, R. Khaledialidusti, W. Hong, M. Sternberg, S. Sankaranarayanan, B. Anasori, *ACS Nano* **2021**, 15, 12815.
- [28] Q. Tao, M. Dahlqvist, J. Lu, S. Kota, R. Meshkian, J. Halim, J. Palisaitis, L. Hultman, M. Barsoum, P. Persson, J. Rosen, *Nat. Commun.* **2017**, 8, 14949.
- [29] L. Dong, H. Kumar, B. Anasori, Y. Gogotsi, V. Shenoy, *J. Phys. Chem. Lett.* **2017**, 8, 422.
- [30] C. Wang, S. Chen, L. Song, *Adv. Funct. Mater.* **2020**, 30, 2000869.
- [31] B. Anasori, M. Lukatskaya, Y. Gogotsi, *Nat. Rev. Mater.* **2017**, 2, 16098.
- [32] S. Naqvi, V. Shukla, N. Jena, W. Luo, R. Ahuja, *Appl. Mater. Today* **2020**, 19, 100574.
- [33] R. Khaledialidusti, A. Mishra, A. Barnoush, *J. Mater. Chem. C* **2020**, 8, 4771.
- [34] T. Mathis, K. Maleski, A. Goad, A. Sarycheva, M. Anayee, A. Foucher, K. Hantanasirisakul, C. Shuck, E. Stach, Y. Gogotsi, *ACS Nano* **2021**, 15, 6420.
- [35] L. Fu, W. Xia, *Adv. Eng. Mater.* **2021**, 23, 2001191.
- [36] J. Gonzalez-Julian, *J. Am. Chem. Soc.* **2020**, 104, 659.
- [37] L. Verger, C. Xu, V. Natu, H. Cheng, W. Ren, M. Barsoum, *Curr. Opin. Solid State Mater. Sci.* **2019**, 23, 149.
- [38] M. Naguib, M. Barsoum, Y. Gogotsi, *Adv. Mater.* **2021**, 33, 2103393.
- [39] X. Jiang, A. Kuklin, A. Baev, Y. Ge, H. Agren, H. Zhang, P. Prasad, *Phys. Rep.* **2020**, 848, 1.
- [40] L. Gao, H. Chen, F. Zhang, S. Mei, Y. Zhang, W. Bao, C. Ma, P. Yin, J. Guo, X. Jiang, S. Xu, W. Huang, X. Feng, F. Xu, S. Wei, H. Zhang, *Small Methods* **2020**, 4, 2000250.
- [41] Y. Zhang, Y. Xu, L. Gao, X. Liu, Y. Fu, C. Ma, Y. Ge, R. Cao, X. Zhang, O. Al-Hartomy, S. Wageh, A. Al-Ghamdi, H. Algarni, Z. Shi, H. Zhang, *Mater. Today Phys.* **2021**, 21, 100479.
- [42] L. Gao, W. Bao, A. V. Kuklin, S. Mei, H. Zhang, H. Agren, *Adv. Mater.* **2021**, 33, 2004129.
- [43] L. Gao, C. Li, W. Huang, S. Mei, H. Lin, Q. Ou, Y. Zhang, J. Guo, F. Zhang, S. Xu, H. Zhang, *Chem. Mater.* **2020**, 32, 1703.
- [44] Y. Liu, P. Zhang, N. Sun, B. Anasori, Q. Zhu, H. Liu, Y. Gogotsi, B. Xu, *Adv. Mater.* **2018**, 30, 1707334.
- [45] X. Xu, Y. Zhang, H. Sun, J. Zhou, F. Yang, H. Li, H. Chen, Y. Chen, Z. Liu, Z. Qiu, D. Wang, L. Ma, J. Wang, Q. Zeng, Z. Peng, *Adv. Electron. Mater.* **2021**, 7, 2000967.
- [46] X. Tang, X. Guo, W. Wu, G. Wang, *Adv. Energy Mater.* **2018**, 8, 1801897.
- [47] Z. Zhang, S. Yang, P. Zhang, J. Zhang, G. Chen, X. Feng, *Nat. Commun.* **2019**, 10, 2920.
- [48] H. Riazi, S. Neman, M. Grady, B. Anasori, M. Soroush, *J. Mater. Chem. A* **2021**, 9, 8051.
- [49] X. Gao, Z. Li, J. Xue, Y. Qian, L. Zhang, J. Caro, H. Wang, *J. Membrane Sci.* **2019**, 586, 162.
- [50] F. Shahzad, M. Alhabeb, C. Hatter, B. Anasori, S. Man Hong, C. Koo, Y. Gogotsi, *Science* **2016**, 353, 1137.
- [51] R. Bian, G. He, W. Zhi, S. Xiang, T. Wang, D. Cai, *J. Mater. Chem. C* **2019**, 7, 474.
- [52] Y. Wan, K. Rajavel, X. Li, X. Wang, S. Liao, Z. Lin, P. Zhu, R. Sun, C. Wong, *Chem. Eng. J.* **2021**, 408, 127303.
- [53] E. Lee, A. VahidMohammadi, Y. Yoon, M. Beidaghi, D. Kim, *ACS Sens.* **2019**, 4, 1603.
- [54] S. Kim, H. Koh, C. Ren, O. Kwon, K. Maleski, S. Cho, B. Anasori, C. Kim, Y. Choi, J. Kim, Y. Gogotsi, H. Jung, *ACS Nano* **2018**, 12, 986.
- [55] M. Wu, M. He, Q. Hu, Q. Wu, G. Sun, L. Xie, Z. Zhang, Z. Zhu, A. Zhou, *ACS Sens.* **2019**, 4, 2763.
- [56] Y. Pei, X. Zhang, Z. Hui, J. Zhou, X. Huang, G. Sun, W. Huang, *ACS Nano* **2021**, 15, 3996.
- [57] Y. Wang, Y. Nian, A. Biswas, W. Li, Y. Han, J. Chen, *Adv. Energy Mater.* **2021**, 11, 2002967.
- [58] Y. Zhao, M. Que, J. Chen, C. Yang, *J. Mater. Chem. C* **2020**, 8, 16258.
- [59] Z. Wu, C. Li, Z. Li, K. Feng, M. Cai, D. Zhang, S. Wang, M. Chu, C. Zhang, J. Shen, Z. Huang, Y. Xiao, G. Ozin, X. Zhang, L. He, *ACS Nano* **2021**, 15, 5696.
- [60] Á. Morales-García, F. Calle-Vallejo, F. Illas, *ACS Catal.* **2020**, 10, 13487.
- [61] I. Chirica, A. Mirea, Ş. Neaţu, M. Florea, M. Barsoum, F. Neaţu, *J. Mater. Chem. A* **2021**, 9, 19589.
- [62] X. Li, Z. Huang, C. Zhi, *Front. Mater.* **2019**, 6, 00312.
- [63] C. Zhang, S. Pinilla, N. McEvoy, C. Cullen, B. Anasori, E. Long, S. Park, A. Seral-Ascaso, A. Shmeliov, D. Krishnan, C. Morant, X. Liu, G. Duesberg, Y. Gogotsi, V. Nicolosi, *Chem. Mater.* **2017**, 29, 4848.
- [64] R. Meshkian, Q. Tao, M. Dahlqvist, J. Lu, L. Hultman, J. Rosen, *Acta Mater.* **2017**, 125, 476.
- [65] O. Mashtalir, K. Cook, V. Mochalin, M. Crowe, M. Barsoum, Y. Gogotsi, *J. Mater. Chem. A* **2014**, 2, 14334.

- [66] J. Li, R. Qin, L. Yan, Z. Chi, Z. Yu, N. Li, M. Hu, H. Chen, G. Shan, *Inorg. Chem.* **2019**, 58, 7285.
- [67] J. Palisaitis, I. Persson, J. Halim, J. Rosen, P. Persson, *Nanoscale* **2018**, 10, 10850.
- [68] T. Habib, X. Zhao, S. Shah, Y. Chen, W. Sun, H. An, J. Lutkenhaus, M. Radovic, M. Green, *npj 2D Mater. Appl.* **2019**, 3, 8.
- [69] H. Shi, P. Zhang, Z. Liu, S. Park, M. Lohe, Y. Wu, A. S. Nia, S. Yang, X. Feng, *Angew. Chem., Int. Ed.* **2021**, 60, 8689.
- [70] M. Li, J. Lu, K. Luo, Y. Li, K. Chang, K. Chen, J. Zhou, J. Rosen, L. Hultman, P. Eklund, P. Persson, S. Du, Z. Chai, Z. Huang, Q. Huang, *J. Am. Chem. Soc.* **2019**, 141, 4730.
- [71] Y. Gogotsi, *Nat. Mater.* **2015**, 14, 1079.
- [72] S. Yang, P. Zhang, F. Wang, A. Ricciardulli, M. Lohe, P. Blom, X. Feng, *Angew. Chem., Int. Ed.* **2018**, 57, 15491.
- [73] O. Mashtalir, M. Naguib, V. Mochalin, Y. Dall'Agnese, M. Heon, M. Barsoum, Y. Gogotsi, *Nat. Commun.* **2013**, 4, 1716.
- [74] O. Mashtalir, M. Lukatskaya, M. Zhao, M. Barsoum, Y. Gogotsi, *Adv. Mater.* **2015**, 27, 3501.
- [75] M. Naguib, R. Unocic, B. Armstrong, J. Nanda, *Dalton Trans.* **2015**, 44, 9353.
- [76] D. Xiong, X. Li, Z. Bai, S. Lu, *Small* **2018**, 14, 1703419.
- [77] M. Hope, A. Forse, K. Griffith, M. Lukatskaya, M. Ghidui, Y. Gogotsi, C. Grey, *Phys. Chem. Chem. Phys.* **2016**, 18, 5099.
- [78] X. Sang, Y. Xie, M. Lin, M. Alhabeb, K. Van Aken, Y. Gogotsi, P. Kent, K. Xiao, R. Unocic, *ACS Nano* **2016**, 10, 9193.
- [79] R. Ronchi, J. Arantes, S. Santos, *Ceram. Int.* **2019**, 45, 18167.
- [80] K. Wang, Y. Zhou, W. Xu, D. Huang, Z. Wang, M. Hong, *Ceram. Int.* **2016**, 42, 8419.
- [81] A. Feng, Y. Yu, Y. Wang, F. Jiang, Y. Yu, L. Mi, L. Song, *Mater. Des.* **2017**, 114, 161.
- [82] A. Lipatov, M. Alhabeb, M. Lukatskaya, A. Boson, Y. Gogotsi, A. Sinitskii, *Adv. Electron. Mater.* **2016**, 2, 1600255.
- [83] C. Shuck, M. Han, K. Maleski, K. Hantanasirisakul, S. Kim, J. Choi, W. Reil, Y. Gogotsi, *ACS Appl. Nano Mater.* **2019**, 2, 3368.
- [84] Y. Tian, W. Que, Y. Luo, C. Yang, X. Yin, L. Kong, *J. Mater. Chem. A* **2019**, 7, 5416.
- [85] M. Ghidui, M. Lukatskaya, M. Zhao, Y. Gogotsi, M. Barsoum, *Nature* **2014**, 516, 78.
- [86] P. Urbankowski, B. Anasori, T. Makaryan, D. Er, S. Kota, P. Walsh, M. Zhao, V. Shenoy, M. Barsoum, Y. Gogotsi, *Nanoscale* **2016**, 8, 11385.
- [87] A. Djire, H. Zhang, J. Liu, E. Miller, N. Neale, *ACS Appl. Mater. Interfaces* **2019**, 11, 11812.
- [88] W. Sun, S. Shah, Y. Chen, Z. Tan, H. Gao, T. Habib, M. Radovic, M. Green, *J. Mater. Chem. A* **2017**, 5, 21663.
- [89] S. Kajiyama, L. Szabova, H. Iinuma, A. Sugahara, K. Gotoh, K. Sodeyama, Y. Tateyama, M. Okubo, A. Yamada, *Adv. Energy Mater.* **2017**, 7, 1601873.
- [90] Y. Li, H. Shao, Z. Lin, J. Lu, L. Liu, B. Duployer, P. Persson, P. Eklund, L. Hultman, M. Li, K. Chen, X. Zha, S. Du, P. Rozier, Z. Chai, E. Raymundo-Pinero, P. Taberna, P. Simon, Q. Huang, *Nat. Mater.* **2020**, 19, 894.
- [91] W. Mounfield, B. Huang, B. Cai, Y. Shao-Horn, Y. Román-Leshkov, *Mater. Lett.* **2020**, 261, 126987.
- [92] C. Xu, L. Wang, Z. Liu, L. Chen, J. Guo, N. Kang, X. Ma, H. Cheng, W. Ren, *Nat. Mater.* **2015**, 14, 1135.
- [93] S. Pang, Y. Wong, S. Yuan, Y. Liu, M. Tsang, Z. Yang, H. Huang, W. Wong, J. Hao, *J. Am. Chem. Soc.* **2019**, 141, 9610.
- [94] M. Zhao, M. Sedran, Z. Ling, M. Lukatskaya, O. Mashtalir, M. Ghidui, B. Dyatkin, D. Tallman, T. Djenizian, M. Barsoum, Y. Gogotsi, *Angew. Chem., Int. Ed.* **2015**, 54, 4810.
- [95] X. Li, M. Li, Q. Yang, G. Liang, Z. Huang, L. Ma, D. Wang, F. Mo, B. Dong, Q. Huang, C. Zhi, *Adv. Energy Mater.* **2020**, 10, 2001791.
- [96] Z. Wu, W. Ren, L. Gao, J. Zhao, Z. Chen, B. Liu, D. Tang, B. Yu, C. Jiang, H. Cheng, *ACS Nano* **2009**, 3, 411.
- [97] Z. Li, L. Wang, D. Sun, Y. Zhang, B. Liu, Q. Hu, A. Zhou, *Mater. Sci. Eng., B* **2015**, 191, 33.
- [98] K. Kim, W. Regan, B. Geng, B. Alemán, B. Kessler, F. Wang, M. Crommie, A. Zettl, *Phys. Status Solidi RRL* **2010**, 4, 302.
- [99] F. Kong, X. He, Q. Liu, X. Qi, Y. Zheng, R. Wang, Y. Bai, *Electrochim. Acta* **2018**, 265, 140.
- [100] M. Seredych, C. Shuck, D. Pinto, M. Alhabeb, E. Precetti, G. Deysher, B. Anasori, N. Kurra, Y. Gogotsi, *Chem. Mater.* **2019**, 31, 3324.
- [101] N. Osti, M. Naguib, M. Tyagi, Y. Gogotsi, A. Kolesnikov, E. Mamontov, *Phys. Rev. Mater.* **2017**, 1, 024004.
- [102] N. Osti, M. Naguib, A. Ostadhossein, Y. Xie, P. Kent, B. Dyatkin, G. Rother, W. Heller, A. van Duin, Y. Gogotsi, E. Mamontov, *ACS Appl. Mater. Interfaces* **2016**, 8, 8859.
- [103] N. Osti, M. Naguib, K. Ganeshan, Y. Shin, A. Ostadhossein, A. van Duin, Y. Cheng, L. Daemen, Y. Gogotsi, E. Mamontov, A. Kolesnikov, *Phys. Rev. Mater.* **2017**, 1, 065406.
- [104] M. Ghidui, S. Kota, V. Drozd, M. Barsoum, *Sci. Adv.* **2018**, 4, eaao6850.
- [105] Y. Xie, M. Naguib, V. Mochalin, M. Barsoum, Y. Gogotsi, X. Yu, K. Nam, X. Yang, A. Kolesnikov, P. Kent, *J. Am. Chem. Soc.* **2014**, 136, 6385.
- [106] Y. Lee, S. Kim, Y. Kim, Y. Lim, Y. Chae, B. Lee, Y. Kim, H. Han, Y. Gogotsi, C. Ahn, *J. Mater. Chem. A* **2020**, 8, 573.
- [107] I. Persson, L. Näslund, J. Halim, M. Barsoum, V. Darakchieva, J. Palisaitis, J. Rosen, P. Persson, *2D Mater.* **2017**, 5, 015002.
- [108] J. Li, Y. Du, C. Huo, S. Wang, C. Cui, *Ceram. Int.* **2015**, 41, 2631.
- [109] Y. Sun, S. Li, Y. Zhuang, G. Liu, W. Xing, W. Jing, *J. Membrane Sci.* **2019**, 591, 117350.
- [110] Z. Zhang, Z. Yao, X. Zhang, Z. Jiang, *Electrochim. Acta* **2020**, 359, 136960.
- [111] I. Persson, J. Halim, T. Hansen, J. Wagner, V. Darakchieva, J. Palisaitis, J. Rosen, P. Persson, *Adv. Funct. Mater.* **2020**, 30, 1909005.
- [112] L. Gan, D. Huang, U. Schwingenschlögl, *J. Mater. Chem. A* **2013**, 1, 13672.
- [113] T. Su, R. Peng, Z. Hood, M. Naguib, I. Ivanov, J. Keum, Z. Qin, Z. Guo, Z. Wu, *ChemSusChem* **2018**, 11, 688.
- [114] W. Yuan, L. Cheng, Y. Zhang, H. Wu, S. Lv, L. Chai, X. Guo, L. Zheng, *Adv. Mater. Interfaces* **2017**, 4, 1700577.
- [115] X. Li, X. Yin, M. Han, C. Song, X. Sun, H. Xu, L. Cheng, L. Zhang, *J. Mater. Chem. C* **2017**, 5, 7621.
- [116] H. Ghassemi, W. Harlow, O. Mashtalir, M. Beidaghi, M. Lukatskaya, Y. Gogotsi, M. Taheri, *J. Mater. Chem. A* **2014**, 2, 14339.
- [117] M. Naguib, O. Mashtalir, M. Lukatskaya, B. Dyatkin, C. Zhang, V. Presser, Y. Gogotsi, M. Barsoum, *Chem. Commun.* **2014**, 50, 7420.
- [118] R. Rakhi, B. Ahmed, M. Hedhili, D. Anjum, H. Alshareef, *Chem. Mater.* **2015**, 27, 5314.
- [119] F. Xia, J. Lao, R. Yu, X. Sang, J. Luo, Y. Li, J. Wu, *Nanoscale* **2019**, 11, 23330.
- [120] C. Zhang, S. Kim, M. Ghidui, M. Zhao, M. Barsoum, V. Nicolosi, Y. Gogotsi, *Adv. Funct. Mater.* **2016**, 26, 4143.
- [121] A. VahidMohammadi, M. Mojtavani, N. Caffrey, M. Wanunu, M. Beidaghi, *Adv. Mater.* **2019**, 31, 1806931.
- [122] D. Hanlon, C. Backes, E. Doherty, C. Cucinotta, N. Berner, C. Boland, K. Lee, A. Harvey, P. Lynch, Z. Gholamvand, S. Zhang, K. Wang, G. Moynihan, A. Pokle, Q. Ramasse, N. McEvoy, W. Blau, J. Wang, G. Abellan, F. Hauke, A. Hirsch, S. Sanvito, D. O'Regan, G. Duesberg, V. Nicolosi, J. Coleman, *Nat. Commun.* **2015**, 6, 8563.
- [123] S. Doo, A. Chae, D. Kim, T. Oh, T. Ko, S. Kim, D. Koh, C. Koo, *ACS Appl. Mater. Interfaces* **2021**, 13, 22855.
- [124] S. Huang, V. Mochalin, *Inorg. Chem.* **2019**, 58, 1958.

- [125] D. Kim, T. Ko, H. Kim, G. Lee, S. Cho, C. Koo, *ACS Nano* **2019**, *13*, 13818.
- [126] Y. Wen, T. Rufford, X. Chen, N. Li, M. Lyu, L. Dai, L. Wang, *Nano Energy* **2017**, *38*, 368.
- [127] W. Bao, L. Liu, C. Wang, S. Choi, D. Wang, G. Wang, *Adv. Energy Mater.* **2018**, *8*, 1702485.
- [128] R. Thakur, A. VahidMohammadi, J. Moncada, W. Adams, M. Chi, B. Tatarchuk, M. Beidaghi, C. Carrero, *Nanoscale* **2019**, *11*, 10716.
- [129] H. Wang, Y. Wu, J. Zhang, G. Li, H. Huang, X. Zhang, Q. Jiang, *Mater. Lett.* **2015**, *160*, 537.
- [130] M. Han, X. Yin, H. Wu, Z. Hou, C. Song, X. Li, L. Zhang, L. Cheng, *ACS Appl. Mater. Interfaces* **2016**, *8*, 21011.
- [131] H. Xu, X. Yin, X. Li, M. Li, L. Zhang, L. Cheng, *Funct. Compos. Struct.* **2019**, *1*, 015002.
- [132] X. Zhao, D. Holta, Z. Tan, J. Oh, I. Echols, M. Anas, H. Cao, J. Lutkenhaus, M. Radovic, M. Green, *ACS Appl. Nano Mater.* **2020**, *3*, 10578.
- [133] K. Maleski, V. Mochalin, Y. Gogotsi, *Chem. Mater.* **2017**, *29*, 1632.
- [134] B. Ahmed, D. Anjum, M. Hedhili, Y. Gogotsi, H. Alshareef, *Nanoscale* **2016**, *8*, 7580.
- [135] H. Tang, S. Zhuang, Z. Bao, C. Lao, Y. Mei, *ChemElectroChem* **2016**, *3*, 871.
- [136] M. Cao, F. Wang, L. Wang, W. Wu, W. Lv, J. Zhu, *J. Electrochem. Soc.* **2017**, *164*, A3933.
- [137] Y. Dong, Z. Wu, S. Zheng, X. Wang, J. Qin, S. Wang, X. Shi, X. Bao, *ACS Nano* **2017**, *11*, 4792.
- [138] X. Zhao, A. Vashisth, J. Blivin, Z. Tan, D. Holta, V. Kotasthane, S. Shah, T. Habib, S. Liu, J. Lutkenhaus, M. Radovic, M. Green, *Adv. Mater. Interfaces* **2020**, *7*, 2000845.
- [139] R. Lotfi, M. Naguib, D. Yilmaz, J. Nanda, A. van Duin, *J. Mater. Chem. A* **2018**, *6*, 12733.
- [140] H. Kim, B. Anasori, Y. Gogotsi, H. Alshareef, *Chem. Mater.* **2017**, *29*, 6472.
- [141] J. Zhou, X. Zha, F. Chen, Q. Ye, P. Eklund, S. Du, Q. Huang, *Angew. Chem., Int. Ed.* **2016**, *55*, 5008.
- [142] M. Ashton, K. Mathew, R. Hennig, S. Sinnott, *J. Phys. Chem. C* **2016**, *120*, 3550.
- [143] J. Halim, K. Cook, M. Naguib, P. Eklund, Y. Gogotsi, J. Rosen, M. Barsoum, *Appl. Surf. Sci.* **2016**, *362*, 406.
- [144] J. Lu, I. Persson, H. Lind, J. Palisaitis, M. Li, Y. Li, K. Chen, J. Zhou, S. Du, Z. Chai, Z. Huang, L. Hultman, P. Eklund, J. Rosen, Q. Huang, P. Persson, *Nanoscale Adv.* **2019**, *1*, 3680.
- [145] A. Iqbal, J. Hong, T. Ko, C. Koo, *Nano Convergence* **2021**, *8*, 9.
- [146] X. Wu, Z. Wang, M. Yu, L. Xiu, J. Qiu, *Adv. Mater.* **2017**, *29*, 1607017.
- [147] Y. Chae, S. Kim, S. Cho, J. Choi, K. Maleski, B. Lee, H. Jung, Y. Gogotsi, Y. Lee, C. Ahn, *Nanoscale* **2019**, *11*, 8387.
- [148] V. Natu, J. Hart, M. Sokol, H. Chiang, M. Taheri, M. Barsoum, *Angew. Chem., Int. Ed.* **2019**, *58*, 12655.
- [149] X. Zhao, A. Vashisth, E. Prehn, W. Sun, S. Shah, T. Habib, Y. Chen, Z. Tan, J. Lutkenhaus, M. Radovic, M. Green, *Matter* **2019**, *1*, 513.
- [150] A. Feng, Y. Yu, F. Jiang, Y. Wang, L. Mi, Y. Yu, L. Song, *Ceram. Int.* **2017**, *43*, 6322.
- [151] N. Caffrey, *Nanoscale* **2018**, *10*, 13520.
- [152] G. Henkelman, A. Arnaldsson, H. Jónsson, *Comp. Mater. Sci.* **2006**, *36*, 354.
- [153] I. Persson, J. Halim, H. Lind, T. Hansen, J. Wagner, L. Naslund, V. Darakchieva, J. Palisaitis, J. Rosen, P. Persson, *Adv. Mater.* **2019**, *31*, 1805472.
- [154] O. Mashtalir, M. Lukatskaya, A. Kolesnikov, E. Raymundo-Pinero, M. Naguib, M. Barsoum, Y. Gogotsi, *Nanoscale* **2016**, *8*, 9128.
- [155] C. Ling, L. Shi, Y. Ouyang, Q. Chen, J. Wang, *Adv. Sci.* **2016**, *3*, 1600180.
- [156] A. Sreedhar, J. Noh, *Sol. Energy* **2021**, *222*, 48.
- [157] S. Cao, B. Shen, T. Tong, J. Fu, J. Yu, *Adv. Funct. Mater.* **2018**, *28*, 1800136.
- [158] Z. Miao, G. Wang, X. Zhang, X. Dong, *Appl. Surf. Sci.* **2020**, *528*, 146929.
- [159] C. Peng, X. Yang, Y. Li, H. Yu, H. Wang, F. Peng, *ACS Appl. Mater. Interfaces* **2016**, *8*, 6051.
- [160] Y. Gao, L. Wang, A. Zhou, Z. Li, J. Chen, H. Bala, Q. Hu, X. Cao, *Mater. Lett.* **2015**, *150*, 62.
- [161] J. Zhang, L. Yang, H. Wang, G. Zhu, H. Wen, H. Feng, X. Sun, X. Guan, J. Wen, Y. Yao, *Inorg. Chem.* **2019**, *58*, 5414.
- [162] T. Hou, Q. Li, Y. Zhang, W. Zhu, K. Yu, S. Wang, Q. Xu, S. Liang, L. Wang, *Appl. Catal., B* **2020**, *273*, 119072.
- [163] H. Wang, R. Peng, Z. Hood, M. Naguib, S. Adhikari, Z. Wu, *ChemSusChem* **2016**, *9*, 1490.
- [164] Y. Xu, S. Wang, J. Yang, B. Han, R. Nie, J. Wang, J. Wang, H. Jing, *Nano Energy* **2018**, *51*, 442.
- [165] J. Zhu, Y. Tang, C. Yang, F. Wang, M. Cao, *J. Electrochem. Soc.* **2016**, *163*, A785.
- [166] J. Low, L. Zhang, T. Tong, B. Shen, J. Yu, *J. Catal.* **2018**, *361*, 255.
- [167] Y. Li, X. Deng, J. Tian, Z. Liang, H. Cui, *Appl. Mater. Today* **2018**, *13*, 217.
- [168] G. Liu, H. Yang, J. Pan, Y. Yang, G. Lu, H. Cheng, *Chem. Rev.* **2014**, *114*, 9559.
- [169] G. Zou, J. Guo, Q. Peng, A. Zhou, Q. Zhang, B. Liu, *J. Mater. Chem. A* **2016**, *4*, 489.
- [170] H. Yang, C. Sun, S. Qiao, J. Zou, G. Liu, S. Smith, H. Cheng, G. Lu, *Nature* **2008**, *453*, 638.
- [171] A. Shahzad, K. Rasool, M. Nawaz, W. Miran, J. Jang, M. Moztahida, K. Mahmoud, D. Lee, *Chem. Eng. J.* **2018**, *349*, 748.
- [172] C. Peng, H. Wang, H. Yu, F. Peng, *Mater. Res. Bull.* **2017**, *89*, 16.
- [173] X. Cheng, L. Zu, Y. Jiang, D. Shi, X. Cai, Y. Ni, S. Lin, Y. Qin, *Chem. Commun.* **2018**, *54*, 11622.
- [174] C. Yang, Y. Tang, Y. Tian, Y. Luo, M. F. Ud Din, X. Yin, W. Que, *Adv. Energy Mater.* **2018**, *8*, 1802087.
- [175] T. Ke, S. Shen, K. Rajavel, K. Yang, D. Lin, *J. Hazard. Mater.* **2021**, *402*, 124066.
- [176] L. Li, G. Jiang, C. An, Z. Xie, Y. Wang, L. Jiao, H. Yuan, *Nanoscale* **2020**, *12*, 10369.
- [177] L. Deng, B. Chang, D. Shi, X. Yao, Y. Shao, J. Shen, B. Zhang, Y. Wu, X. Hao, *Renewable Energy* **2021**, *170*, 858.
- [178] W. Gao, X. Li, S. Luo, Z. Luo, X. Zhang, R. Huang, M. Luo, *J. Colloid Interface Sci.* **2021**, *585*, 20.
- [179] Q. Yin, Z. Cao, Z. Wang, J. Zhai, M. Li, L. Guan, B. Fan, W. Liu, G. Shao, H. Xu, H. Wang, R. Zhang, H. Lu, *Nanotechnology* **2021**, *32*, 015706.
- [180] Y. Li, Z. Yin, G. Ji, Z. Liang, Y. Xue, Y. Guo, J. Tian, X. Wang, H. Cui, *Appl. Catal., B* **2019**, *246*, 12.
- [181] Y. Li, L. Ding, Z. Liang, Y. Xue, H. Cui, J. Tian, *Chem. Eng. J.* **2020**, *383*, 123178.
- [182] K. Huang, C. Li, X. Meng, *J. Colloid Interface Sci.* **2020**, *580*, 669.
- [183] N. Hao, Y. Wei, J. Wang, Z. Wang, Z. Zhu, S. Zhao, M. Han, X. Huang, *RSC Adv.* **2018**, *8*, 20576.
- [184] X. Zhang, J. Li, J. Li, L. Han, T. Lu, X. Zhang, G. Zhu, L. Pan, *Chem. Eng. J.* **2020**, *385*, 123394.
- [185] J. Li, S. Wang, Y. Du, W. Liao, *Ceram. Int.* **2018**, *44*, 7042.
- [186] H. Huang, Y. Song, N. Li, D. Chen, Q. Xu, H. Li, J. He, J. Lu, *Appl. Catal., B* **2019**, *251*, 154.
- [187] Q. Liu, L. Ai, J. Jiang, *J. Mater. Chem. A* **2018**, *6*, 4102.
- [188] M. Liang, X. Bai, F. Yu, J. Ma, *Nano Res.* **2021**, *14*, 684.
- [189] Y. Fang, R. Hu, B. Liu, Y. Zhang, K. Zhu, J. Yan, K. Ye, K. Cheng, G. Wang, D. Cao, *J. Mater. Chem. A* **2019**, *7*, 5363.
- [190] N. Zhao, Y. Hu, J. Du, G. Liu, B. Dong, Y. Yang, J. Peng, J. Li, M. Zhai, *Appl. Surf. Sci.* **2020**, *530*, 147247.
- [191] C. Zhang, M. Beidaghi, M. Naguib, M. Lukatskaya, M. Zhao, B. Dyatkin, K. Cook, S. Kim, B. Eng, X. Xiao, D. Long, W. Qiao, B. Dunn, Y. Gogotsi, *Chem. Mater.* **2016**, *28*, 3937.



Fangcheng Cao received her Ph.D. in material science and engineering from Shanghai Jiao Tong University in 2018. She is a Teacher at the School of Chemistry and Chemical Engineering of University of South China, Hengyang, China. Her current research interests focus on the development of MAX and MXene materials and their applications in radioactive waste treatment.



Ye Zhang received his Ph.D. in applied chemistry at Soochow University in 2018. He is currently a Professor in the School of Chemistry and Chemical Engineering at University of South China, Hengyang, China. His research interests focus on the development of novel 2D materials and their derived nanodevices.



Hongqing Wang received his Ph.D. in applied chemistry at Central China Normal University in 2004. He is a Professor in the School of Chemistry and Chemical Engineering at University of South China, Hengyang, China. His current research interests focus on the development of novel 2D materials for effective detection and remediation of environmental pollutants.



Karim Khan got his Ph.D. from the Chinese Academy of Sciences in 2016 and worked as a Postdoctoral Researcher at Shenzhen University. Currently he is an Associate Professor in Dongguan University of Technology. His current research focuses on 2D electrocatalyst materials and their applications in energy generation, storage, sensing devices, and biological applications.



Ayesha Khan Tareen earned her Ph.D. (Physical chemistry/Materials) from Ningbo Institute of Material Technology and Engineering, Chinese Academy of Sciences. Currently she is a Postdoctoral Fellow in Shenzhen University. Her research interests include the production of 2D materials and transition metal nitride materials, as well as, their applications in many fields, such as, magnetic materials, photo (electro)-catalysts, fuel cells, and dye-sensitized solar cells.



Wenjing Qian received his Ph.D. degree in applied chemistry at Soochow University. He is currently a Postdoctoral Researcher in the School of Materials Science and Engineering, Tongji University. His research interests mainly focus on the development of 2D materials for energy storage.



Han Zhang is currently a Full Professor in the College of Physics and Optoelectronic Engineering at Shenzhen University in China. He is interested in the development of novel 2D materials and their applications in optoelectronics, bio-medicine, and energy storage.



Hans Ågren is a Professor at the Department of Physics and Astronomy, Uppsala University. His research activities concern molecular/nano/bio photonics and electronics, computational nanoand bio-technology, being a mix of method development and problem-oriented applications.